**Forschungszentrum Karlsruhe**
in der Helmholtz-Gemeinschaft

**Wissenschaftliche Berichte**
FZKA 7409

# Towards the Formulation of a Realistic 3D Model for Simulation of Magnetron Injection Guns for Gyrotrons

## (A Preliminary Study)

**S. Sabchevski, S. Illy, B. Piosczyk, E. Borie, I. Zhelyazkov**

**Institut für Hochleistungsimpuls-und Mikrowellentechnik**
**Programm Kernfusion**
**Association EURATOM/Forschungszentrum Karlsruhe**
**Association EURATOM/INRNE-BG**

**Juli 2008**

**Forschungszentrum Karlsruhe**
in der Helmholtz-Gemeinschaft
Wissenschaftliche Berichte
FZKA 7409

# Towards the Formulation of a Realistic 3D Model for Simulation of Magnetron Injection Guns for Gyrotrons (A Preliminary Study)

S. Sabchevski[1], S. Illy, B. Piosczyk, E. Borie, I. Zhelyazkov[2]

Institut für Hochleistungsimpuls-
und Mikrowellentechnik
Programm Kernfusion
Association EURATOM/FZK und
Association EURATOM/INRNE-BG

[1]Institute of Electronics, Bulgarian Academy of Sciences, BG-1784 Sofia
[2]Faculty of Physics, Sofia University, BG-1164 Sofia

**Forschungszentrum Karlsruhe GmbH, Karlsruhe**
**2008**

Forschungszentrum Karlsruhe GmbH
Postfach 3640, 76021 Karlsruhe

Mitglied der Hermann von Helmholtz-Gemeinschaft
Deutscher Forschungszentren (HGF)

ISSN 0947-8620

urn:nbn:de:0005-074094

# Towards the Formulation of a Realistic 3D Model for Simulation of Magnetron Injection Guns for Gyrotrons (A Preliminary Study)

**Abstract**

Numerical experiments based on adequate, self-consistent physical models implemented in simulation codes are widely used for computer-aided design (CAD), analysis and optimization of the electron optical systems (EOS) of the gyrotrons. An essential part of the physical model is the emission model, i.e., the relations that govern the value of the beam current extracted from the emitter as well as its energy spectrum, spatial and angular distribution. In this paper, we present a compendium of the basic theory, the most essential formulas and discuss the most important factors responsible for the nonuniformity of the emission and velocity spread. We also review the emission models realized in various ray-tracing and Particle-In-Cell (PIC) codes and present a general formulation of a 3D emission model based on the principle of decomposition of the region near the cathode to a set of equivalent diodes. It is believed that the information summarized in this compendium will be helpful for the development of novel modules for calculation of the initial distribution in both the available 2D computer programs that are being upgraded now and in the novel 3D simulation tools development of which is in progress now.

# Fortschritte in der Formulierung eines realistischen 3D-Modells für die Simulation von Elektronenkanonen für Gyrotrons (Eine vorläufige Studie)


### Zusammenfassung

Numerische Experimente, die auf adäquaten, selbst-konsistenten physikalischen Modellen basieren, werden in einem breiten Umfang für das computerunterstützte Design (CAD), die Analyse und Optimierung von elektronenoptischen Systemen von Gyrotrons eingesetzt.

Ein wesentlicher Teil des benötigten physikalischen Modells ist das Emissionsmodell, d.h. die Beschreibung des vom Emitter erzeugten Strahlstroms sowie die Energieverteilung und die räumliche und winkelabhängige Verteilung der emittierten Elektronen.

In dieser Arbeit präsentieren wir eine Zusammenfassung der grundlegenden Theorie, die wesentlichen Formeln und eine Diskussion der wichtigsten Faktoren für die Inhomogenität der Emission und der Geschwindigkeitsstreuung. Zusätzlich wird ein Überblick über die in verschiedenen Ray-Tracing und Particle-In-Cell (PIC) Codes eingesetzten Emissionsmodelle geliefert und eine allgemeine Formulierung eines dreidimensionalen Emissionsmodells präsentiert, das auf der Zerlegung der kathodennahen Region durch eine Anzahl entsprechender Diodensegmente basiert.

Wir glauben, dass diese Zusammenfassung bei der Entwicklung neuer Programm-Module zur Berechnung der Elektronen-Anfangsverteilung sehr hilfreich sein wird. Damit können sowohl bereits existierende zweidimensionale Computerprogramme, als auch neu zu entwickelnde dreidimensionale Simulationswerkzeuge ausgestattet werden.

# Contents

# 1 Introduction

Numerical codes for simulation of the electron-optical systems (EOS) of gyrotrons are indispensable tools for analysis, computer aided design (CAD) and optimization of high-performance devices. Currently, most of the available programs are based on 2D self-consistent physical models. At the same time, work on the development of novel numerical packages employing 3D physical models is in progress now (Sabchevski, Zhelyazkov, Thumm, Illy, Piosczyk, Tran, Hogge, and Pagonakis 2007). The emission model implemented in any such code is of critical importance for the adequacy of the simulations as a whole. While the rest of the model (relativistic equations of motion coupled with an appropriate boundary value problem for the self-consistent electromagnetic fields, including the self fields of the space-charge flow) is almost standardized and considered as an essential component of the paradigm of modelling and simulation of magnetron injection guns (MIG) for gyrotrons, the emission model itself is often highly idealized or even neglected. In most of the available computer ray tracing and PIC codes this model is known as "a zero initial emittance of the electron beam" since the macro-particles representing the beam are emitted with zero initial velocities and perpendicular to the cathode and carry equal space charge. Even if in codes where the possibility to specify more realistic initial conditions is left to the user, as a rule the simulations are performed for uniform distribution with zero initial energies. One reason for this is that the straightforward tracing of a large ensemble of particles with distributed initial conditions increases considerably the required computational resources. Many recent studies have shown that such idealization excludes significant physical factors from the numerical experiments. Among them are the nonuniformity of the emission (due to variations of: the surface temperature of the emitter; the work function, the local extracting electron field etc.), energy spectrum of the emitted electrons, time dependence of the emission characteristics of the cathode, surface roughness, magnetic field of the heating filament, and edge effects. The importance of these factors has been demonstrated in a number of numerical simulations and experimental investigations. Here we intend to provide a comprehensive review of the literature on this topic and to collect the most relevant formulas and relations in a compendium which could be useful in the numerical implementation of various emission models in both the currently used codes and the novel codes that are under development at present.

The review is organized as follows. In the next section we recall the well-known theory of the thermionic emission. Some recent contributions to this classical field are also mentioned briefly. In Sec. 3 we present the current status of the technology for manufacturing efficient cathodes for gyrotrons. The sources of the emission nonuniformity and velocity spread in the extracted electron beams are discussed in Sec. 4. The influence of the azimuthal beam nonuniformity and the velocity spread on the overall performance of the tube is considered in Sec. 5. It should be mentioned that there is vast literature on the latter topic. Here we do not try to be exhaustive in reviewing it but rather present the main arguments that substantiate the necessity to take into account these factors in the numerical simulations. Different emission models and their numerical implementation in various computer codes are presented and discussed in Sec. 6. The focus in this section is on the variety of the approaches. That is why we review not only the most advanced and/or widely known codes but also the programs that exploit original or sometimes simply interesting approaches. In the case however, that some model is realized in a series of codes only the most characteristic (or widely known) is presented. In Sec. 7 we outline the prospective general formulation of an emission model that is pertinent for 3D and 2D models. Some conclusions and an outlook are presented in Sec. 8.

A comment about notation seems to be in order here. Whenever possible the original notations of the cited papers are preserved. As a result most of them are locally defined in the corresponding sections. At the same times, if some notation is used through several sections it is described only after its first appearance. In order to be as close as possible to the original formulations given by the authors of the reviewed papers they are cited literally in many cases although this is not always indicated implicitly by quotation marks.

# 2 Basic theory of the emission models

Assumption of a Fermi–Dirac distribution of the carriers in the emitting materials leads to the well-known relations for various emission mechanisms (Hawkes and Kasper 1989). The governing relation for the saturated current of the thermionic emission is the Richardson–Laue–Dushman equation

$$J_{\rm sat} = \frac{4\pi mek_{\rm B}^2T^2}{h^3}e^{-\varphi/k_{\rm B}T}e^{\sqrt{eE/\pi\varepsilon_0}/k_{\rm B}T} = AT^2e^{-\varphi/k_{\rm B}T}e^{\sqrt{eE/\pi\varepsilon_0}/k_{\rm B}T}, \tag{1}$$

where $T$ is the absolute temperature in Kelvin, $\varphi$ is the work function in eV, $E$ is the applied external electric field in $\mathrm{V\,cm^{-1}}$, $k_{\rm B} = 8.617 \times 10^{-5}$ in $\mathrm{eV\,K^{-1}}$ is Boltzmann's constant,

$$A = \frac{4\pi mek_{\rm B}^2T^2}{h^3} = 120.1735\ \mathrm{A\,cm^{-2}K^{-2}}$$

is *Richardson's* constant, $e$ is the elementary electric charge, $m$ is the mass of an electron, $h$ is Planck's constant, and $\varepsilon_0$ is the permittivity of vacuum. With these constants taken into account the above equation can be rewritten in a form that is more convenient for calculations

$$J_{\rm sat} = 120T^2e^{-11605\varphi/T}e^{4.4\sqrt{E}/T}. \tag{2}$$

The second exponential term in these equations accounts for the enhancement of the thermionic emission by the electric field known as the Schottky effect. For the usual conditions at which the thermionic cathodes in MIG for gyrotrons are applied this effect is not significant (for example, large external fields of the order of $1\ \mathrm{V\,\mu m^{-1}}$ are required to increase the emission about 1.5 times) for smooth surfaces. Surface roughness however could lead to high local field enhancement for which this effect could increase the emission dramatically.

In order to study the energy spectrum and the angular distribution of the emitted electrons it is convenient to introduce polar coordinates in momentum space according to the relations

$$\begin{aligned} p_x &= \sqrt{2mE}\sin\gamma\cos\theta, \\ p_y &= \sqrt{2mE}\sin\gamma\sin\theta, \\ p_z &= \sqrt{2mE}\cos\gamma. \end{aligned} \tag{3}$$

Here $p_x$, $p_y$, and $p_z$ are the components of the momentum in a Cartesian coordinate system, $E$ is the total energy of the emitted electron, $\gamma$ is the angle of emission with respect to the outer normal to the cathode surface, and $\theta$ is the azimuthal coordinate. Accordingly, the elementary volume in the momentum space has the form

$$d^3p = p^2\,dpd\Omega = m\sqrt{2mE}\sin\gamma\,dEd\gamma d\theta, \tag{4}$$

where $d\Omega = \sin\gamma\, d\gamma d\theta$ is the element of solid angle. This yields for the elementary current density in polar coordinates

$$d^3J = \frac{4em}{h^3} E \exp\left(-\frac{E+\varphi}{k_\mathrm{B}T}\right) \sin\gamma\cos\gamma\, dE d\gamma d\theta. \tag{5}$$

An integration over all possible angles of emission ($0 \leqslant \theta \leqslant 2\pi$, $0 \leqslant \gamma \leqslant \pi/2$) gives for the distribution of energies

$$dJ = AE \exp\left(-\frac{E+\varphi}{k_\mathrm{B}T}\right) dE. \tag{6}$$

It should be noted that the mean energy of the emitted electrons is $\langle E\rangle = 2k_\mathrm{B}T$ with dispersion $\Delta E = \left(\langle E^2\rangle - \langle E\rangle^2\right)^{1/2} = \sqrt{2}k_\mathrm{B}T$. Another characteristic value (which should not be misinterpreted as a certain mean value) is the most probable energy $E_\mathrm{m} = k_\mathrm{B}T$ corresponding to the maximum of the distribution.

Analogously, integrating over all positive energies at constant values of the emission angle, one can obtain a Lambert-type law for the angular distribution of the emitted current density

$$B(\gamma) = \frac{dJ}{d\Omega} = \frac{1}{\pi} J \cos\gamma. \tag{7}$$

Recently a general electron emission equation has been derived, which accounts for both thermal and field emission (Jensen and Cahay, 2006). In a more compact form it can be written in the following way

$$J(T, E_o, \beta_T, \beta_F) = A_\mathrm{RLD} T^2 N(n, s, u). \tag{8}$$

where $A_\mathrm{RLD} \equiv A = 120.1735\ \mathrm{A\,cm^{-2}K^{-2}}$ is Richardson's constant,

$$N(n, s, u) = n \int_{-\infty}^{u} \frac{\ln\left[1 + e^{n(z-s)}\right]}{1 + e^z} dz, \tag{9}$$

$\beta_T$ is the inverse temperature $1/(k_\mathrm{B}T)$, $\beta_F$ being analogous to $\beta_T$ is a slope factor that depends on the applied electric field, and $E_o$ is an expansion point of the energy component $E_x$ directed at the emission barrier (i.e., $E_x = p_x^2/2m$, where $p_x$ is the $x$ component of the momentum). The arguments of $N(n, s, u)$ are given by $n = \beta_T/\beta_F$, $s = \beta_F(E_o - \mu)$, and $u = \beta_F E_o$, where $\mu$ is the chemical potential (equal to the Fermi energy at zero temperature) of the emitting material measured with respect to the bottom of the conduction band. For a typical dispenser cathode $ns \approx \beta_T\left(\varphi - \sqrt{4QF}\right) \equiv \beta_T\phi \approx 16$ at conditions for thermionic emission ($T = 1150\ ^\circ\mathrm{C}$, $\varphi = 2.1$ eV, $F = 0.01\ \mathrm{eV\,nm^{-1}}$), where $Q = e^2/16\pi\varepsilon_0 = 0.359\,991\ \mathrm{eV\,nm}$, and $\phi$ is the height of the potential barrier above the chemical potential $\mu$. The above formulation goes beyond the well-known generalization for the current density

$$J = A_\mathrm{RLD}(T + cF)^2 \exp[-B(T + cF)], \tag{10}$$

where $F$, as above, is the product of the electron charge and the applied electric field, and $c$, $B$ are constants.

An advantage of the novel general equation is that different regimes are naturally distinguished according to the parameter $n = \beta_T/\beta_F$ (rather than $T + cF$), notably $n > 1$ for field emission and $n < 1$ for thermal emission. Accordingly, the "revised" Fowler–Nordheim

(FN) and Richardson–Laue–Dushman (RLD) formulas for the field dominated emission and for temperature dominated emission are given as follows:

$$J_{\mathrm{FN}} \Rightarrow A_{\mathrm{RLD}}(k_{\mathrm{B}}\beta_F)^{-2}\left[1+\frac{\pi^2}{6}\left(\frac{\beta_F}{\beta_T}\right)^2+\frac{7\pi^4}{360}\left(\frac{\beta_F}{\beta_T}\right)^4\right]\exp\left[\beta_F(\mu-E_o)\right] \tag{11}$$

and

$$J_{\mathrm{RLD}} \Rightarrow A_{\mathrm{RLD}}(k_{\mathrm{B}}\beta_T)^{-2}\left[1+\frac{\pi^2}{6}\left(\frac{\beta_T}{\beta_F}\right)^2+\frac{7\pi^4}{360}\left(\frac{\beta_T}{\beta_F}\right)^4\right]\exp\left[\beta_T(\mu-E_o)\right], \tag{12}$$

respectively. It is crucial to emphasize in Eqs. (11) and (12) that the term $E_o$ is a function of both the field and temperature, and that $E_o(n<1)$ is not the same as $E_o(n>1)$. These two equations definitely give a better insight into the connection (symmetry) between the thermionic and field emission.

Keeping only the leading terms, Eq. (12) takes the form

$$J_{\mathrm{emission}}(F,T) = A_{\mathrm{RLD}}T^2\left(1+\frac{\pi^2}{6}n^2\right)\exp[-(\varphi-\sqrt{4QF})/k_{\mathrm{B}}T], \tag{13}$$

where $n(F,T)=(2/\pi)(h^2/2m)^{1/2}(F^3/Q)^{1/4}/k_{\mathrm{B}}T$.

In the case of space charge limited (SL) emission a potential minimum (virtual cathode) forms in close proximity to the emitting surface with a potential $V_{\min}$. It acts as an energy filter; thus only those electrons that have velocity normal to the cathode greater than $\sqrt{2eV_{\min}/m}$ can pass the plane of potential minimum and proceed to the anode. Electrons which are emitted with smaller velocities return to the cathode. As a result the actual current density $J_{\mathrm{SL}}$ is less than the saturation current density [also known as temperature limited (TL) current density] $J_{\mathrm{TL}}$ and is given by

$$J_{\mathrm{SL}} = J_{\mathrm{TL}}\exp\left(eV_{\min}/k_{\mathrm{B}}T\right) = J_{\mathrm{TL}}\exp\left(11.6\times10^3V_{\min}/T\right). \tag{14}$$

The value of the potential minimum with respect to the cathode is

$$V_{\min} = -\frac{k_{\mathrm{B}}T}{e}\ln\left(\frac{J_{\mathrm{TL}}}{J_{\mathrm{SL}}}\right). \tag{15}$$

Ignoring the initial velocities of emitted electrons and the edge effects (i.e., considering a 1D model of a diode with two infinite parallel electrodes) one can easily re-derive analytically Child's law for the cathode current density in a planar diode which is

$$J_{\mathrm{SL}} = \frac{4\varepsilon_0\sqrt{2e/m}}{9}V^{3/2}/d^2 = 2.335\times10^{-6}V^{3/2}/d^2, \tag{16}$$

where $d$ is the distance between the cathode and the anode.

More detailed solution, which takes into account the initial velocities of the electrons, was obtained by Langmuir and Compton (1931). It can be found in both tabulated form as well as in the form of approximate series expansions. It gives for the current density the following relation (Amboss 1993):

$$J_{\mathrm{SL}} = 2.335\times10^{-6}\frac{(V-V_{\min})^{3/2}}{(z-z_{\min})^2}\left\{1+2.865\left[\frac{k_{\mathrm{B}}T}{e(V-V_{\min})}\right]^{1/2}\right\}. \tag{17}$$

It should be noted that Child's law is derived assuming zero electric field at the emitter. If the cathode is heated at elevated temperatures for which the electrons are produced at a greater rate than can be drawn off, a small retarding field develops and then the above equation holds. If, however, the cathode does not emit enough electrons, an accelerating field is produced which increases the emission (Schottky effect). The condition of zero electric field at the cathode corresponds to the case where the space charge limited emission current density $J_{\mathrm{SL}}$ just equals the temperature limited $J_{\mathrm{TL}}$ value. The critical operating temperature $T_{\mathrm{o}}$ can therefore be computed from the relationship

$$2.335 \times 10^{-6} V_{\mathrm{a,o}}^{3/2}/d^2 = 120 \exp(-11.6 \times 10^3 a) T_{\mathrm{o}}^2 \exp(11.6 \times 10^3 \varphi / T_{\mathrm{o}}), \tag{18}$$

given the diode spacing $d$, anode voltage of the diode $V_{\mathrm{a,o}}$, and the work function $\varphi_{\mathrm{o}}$ of the emitter. Here $a$ is the constant in the temperature dependence of $\varphi$, e.g., $\varphi = \varphi_{\mathrm{o}} + aT$.

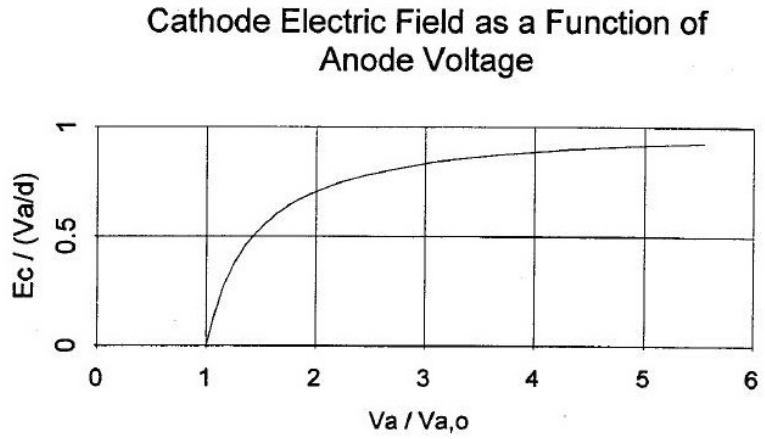


Figure 1: Electric field $E_{\mathrm{c}}$ normalized to the space-charge free electric field, $V_{\mathrm{a}}/d$, as a function of the voltage $V_{\mathrm{a}}$ on the anode normalized to the voltage $V_{\mathrm{a,o}}$ [from (Amboss 1993)].

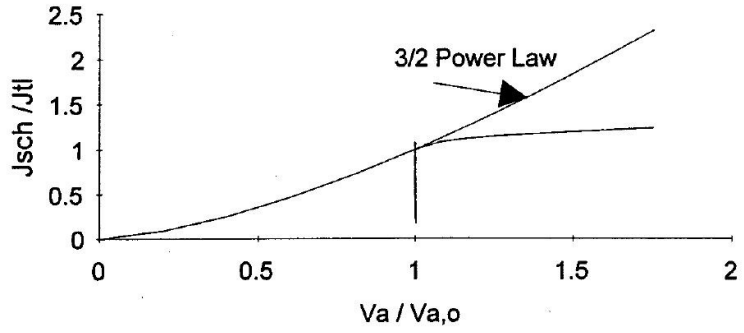


Figure 2: Schottky emission current density $J_{\mathrm{SCH}}$ normalized to the temperature limited emission current density, $J_{\mathrm{TL}}$, as a function of the normalized anode voltage [from (Amboss 1993)].

If the anode voltage $V_{\rm a}$ is increased above $V_{\rm a,o}$, an electric field $E_{\rm c}$ appears at the cathode, which increases the emission density from $J_{\rm TL}$ to $J_{\rm SCH}$ (Schottky effect)

$$J_{\rm SCH} = J_{\rm TL} \exp(0.4 E_{\rm c}^{1/2}/T_{\rm o}). \tag{19}$$

In this case, the electric field can be calculated from the relation (obtained by integrating the Poisson equation with $J_{\rm SCH}$ in its RHS)

$$\left[V_{\rm a}^{1/2} + \frac{1}{B^2}\frac{E_{\rm c}^2}{J_{\rm SCH}}\right]^{3/2} - \frac{3}{B^2}\frac{E_{\rm c}^2}{J_{\rm SCH}}\left[V_{\rm a}^{1/2} + \frac{1}{B^2}\frac{E_{\rm c}^2}{J_{\rm SCH}}\right]^{1/2} + \frac{2}{B^3}\frac{E_{\rm c}^2}{J_{\rm SCH}^{3/2}} = \frac{3}{4} B\, J_{\rm SCH}^{1/2} d \tag{20}$$

for the anode potential at $z = d$.

The above equation can be solved for $V_{\rm a}$ for a specific diode configuration given the voltage $V_{\rm a,o}$ and work function parameters, by assuming a number of $E_{\rm c}$ values. Figure 1 is a plot of $E_{\rm c}$ (when the space charge is absent) normalized to the uniform electric field $V_{\rm a}/d$ as a function of $V_{\rm a}$ normalized to $V_{\rm a,o}$ [for the parameters at which the calculations are made, see Amboss (1993)]. It shows that space charge still affects the electric field of the cathode even when $V_{\rm a}$ exceeds $V_{\rm a,o}$ by a factor of 5.

Figure 2 is a plot of the current density as a function of the normalized anode voltage. One can see that the curve follows the 3/2-power law below $V_{\rm a}/V_{\rm a,o} = 1$. In real cathodes there is always some variation of the work function over the surface of the emitter. The exponential dependence of the temperature limited emission on the work function translates a relatively small spread in the work function into large emission density variations. The effect of this emission density variation is a departure from the 3/2 power law for space charge limited operation since some portions of the cathode become temperature limited while others are still space charge limited. An illustrative example is shown in Fig. 3.

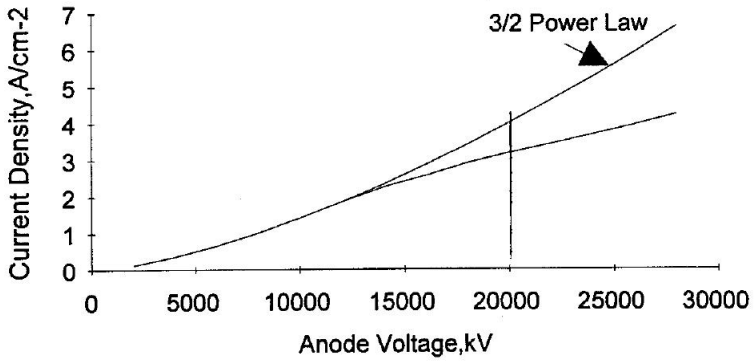


Figure 3: Departure from the 3/2 power law (lower curve) due to portions of the cathode progressively becoming temperature limited owing to work function variations [from (Amboss 1993)].

Recently Longo (2003) proposed an improved interpolation for the transition region between the space charge limited and temperature limited emission

$$\frac{1}{J^\alpha} = \frac{1}{J_{\rm SL}^\alpha} + \frac{1}{J_{\rm TL}^\alpha}, \tag{21}$$

where $\alpha$ is a shape factor (see Figs. 4 and 5).

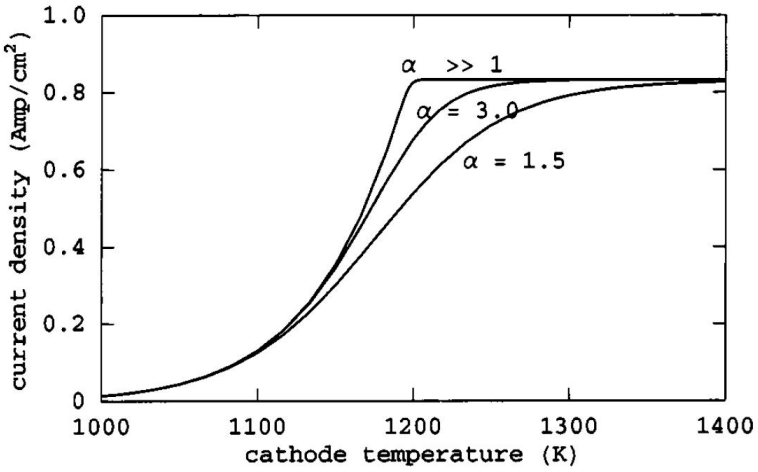


Figure 4: Sensitivity of the emission curve, Eq. (21), to the shape factor $\alpha$. The work function and current loading (i.e., the space charge current) are the same for each curve [from (Longo 2003)].

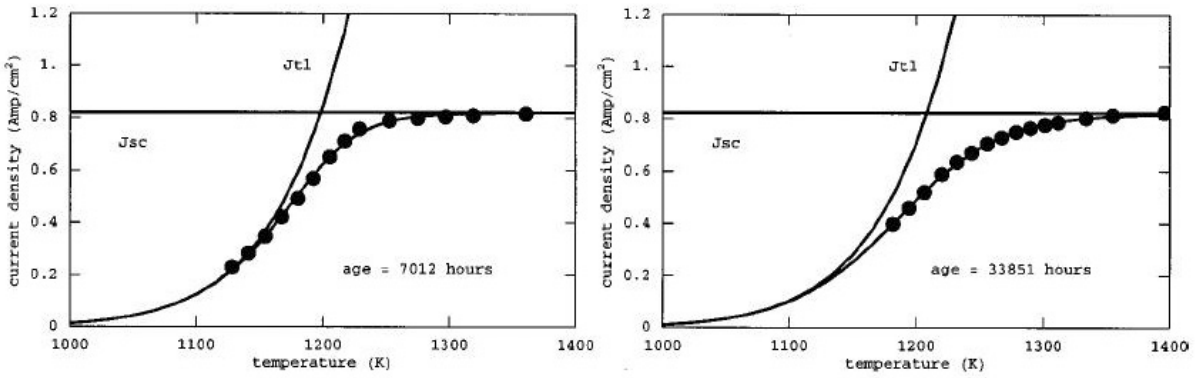


Figure 5: Change of the emission curves due to aging of the cathode [from (Longo 2003)].

As already mentioned, a MIG usually operates in the TL regime. Utilization of the SL mode however is possible and, moreover, it is an appealing alternative, which could solve some of the problems pertaining to the TL emission. This possibility was studied in detail by Lawson, Raghunathan, and Esteban (2004) and by Raghunathan and Lawson (2005). It has been demonstrated that using a space-charge-limited (SCL) MIG it is possible to eliminate the azimuthal current nonuniformity. It has been demonstrated that a comparable beam quality parameters as in a TL MIG could be obtained at the cost of increased peak electric field and emitted current density (cathode loading). Since in a SCL mode the beam current cannot be controlled by varying the cathode temperature, additional control electrodes are introduced for this purpose.

# 3 Cathodes used in the MIG for gyrotrons

Most often, the emitters used in a MIG for gyrotrons are tungsten dispenser cathodes (En-Qiu 1985) produced by compressing and sintering a tungsten powder into cylindrical billets from which a conical emitting section is manufactured. The porous tungsten matrix is impregnated with a mixture consisting of barium oxide (BaO), calcium oxide (CaO), and aluminium oxide ($Al_2O_3$). The composition of these components in a proportion 5:3:2 is known as B-type and in a proportion 4:1:1 as S-type. In so-called M-type dispersion cathodes an additional coating with Os, Ir or Re is used to lower further the work function. The heating of the cathode during its operation causes migration of the barium towards the emitting surface where it lowers the work function.

Early in the life of the cathode, the barium diffusion rate towards the surface can exceed what is required for monolayer coverage. If more than a monolayer of barium atoms builds on the surface of a dispenser cathode, bulk evaporation occurs and is a thermally regulated phenomenon. Removal of Ba from the surface is due to evaporation and ion bombardment (see Fig. 6). Both factors determine the lifetime of the cathode. It was found that initial activation of the barium cathode requires only several hours but in the first 1000 h of life after activation, significant changes occur. The surface itself resembles a porous metal matrix, in which the grains average 4–5 μm in diameter. The pores from which the barium atoms emerge are approximately an average of 2 μm in diameter, and the pore-to-pore separation is approximately 6 μm (Jensen, Lau, and Levush 2000).

It is well known, however, that the main factor that affects the lifetime of the emitter is the cathode loading. Therefore, there is always a trade off between the extracted current and the lifetime (Fig. 7).

Although M-type cathodes coated with Os/Ru or Ir have superior emission characteristics compared to B-type and S-type they are more susceptible to gas poisoning. For such high current emitters emission cooling effects can occur, which lower the temperature of the emitter (Isagawa, Higuchi, Kobayashi, Miyake, Ohya, and Yoshida 1999).

One of the latest advanced cathodes is the so-called Control Porosity Dispenser (CPD) cathode in which a thin (20–30 μm) tungsten film is used. In this film regularly arranged holes several millimeters in diameter are drilled by a laser beam. While the work function of a standard CPD cathode is around 2.0 eV, when covered by Os/Ru it is reduced to about 1.8 eV.

Another very promising (though not yet widely available) novel type of cathode is the *Scandate cathode*, which offers saturated current density as high as several hundred amperes per square centimeter. The Barium Scandate cathode employs scandium oxide ($Sc_2O_3$) to lower the work function of the emissive surface. As a result, this emitter may be operated at lower temperatures than the standard dispenser cathode for the same current density. Since the Barium Scandate mix is homogeneous throughout the tungsten matrix, it is free of many of the problems associated with thin film coated emitters. One distinct advantage over thin film types such as the M-cathode is the ability of the Barium Scandate cathode to withstand much greater levels of ion bombardment before surface sputtering becomes a problem. Other advantages of the Barium Scandate cathode include excellent resistance to possible surface abrasions encountered during inspection, packaging, jigging and general handling, as well as increased resistance to exposure to moisture (HeatWave Labs, Inc. 2001).

Both the design and the machining of the cathode should secure: (i) a smooth emitting surface, (ii) a uniform work function, (iii) uniform heating (within few degrees over the entire

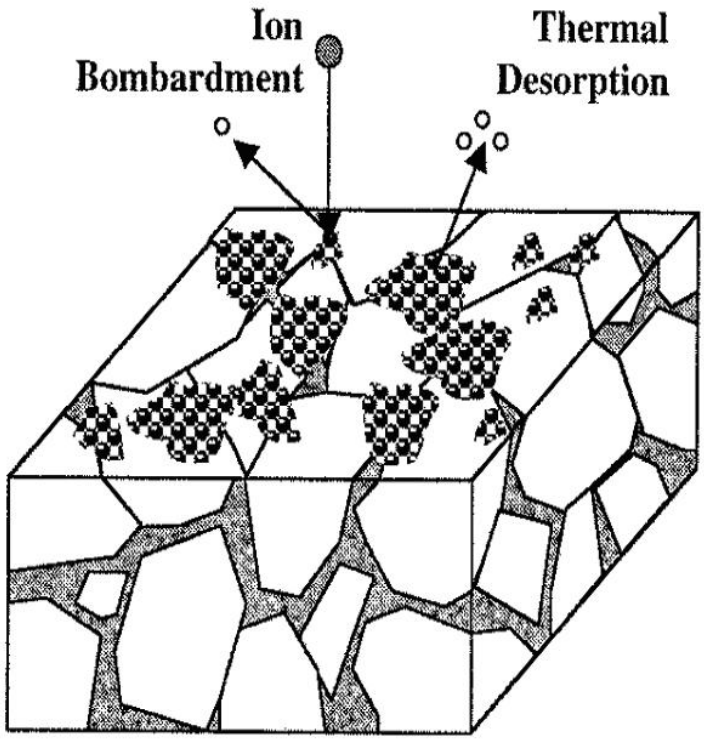


Figure 6: Schematic of cathode surface. The large blocks are tungsten grains of average size 4.5 μm. The separation between pores averages 6 μm, and the pore diameter averages 2–3 μm. In the "Thermal Desorption" regions barium evaporates from the surface. In the "Ion Bombardment" regions barium is sputtered off [from (Jensen, Lau, and Levush 2000)].

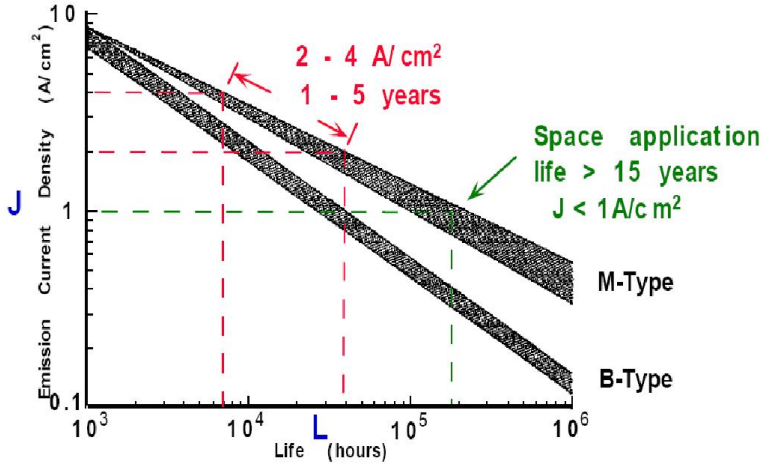


Figure 7: Lifetime of the cathode and a trade-off between lifetime and extracted current [from (Gilmour 1986)].

surface), (iv) thermal stability that prevents a temperature drift of the configuration (distortions, buckling and creasing) and parameters of the emitter with time, and (v) uniform distribution of the electric field over the emitter. The first two requirements cannot be satisfied easily due to the porosity. The later can be controlled to a certain extent by the initial grain size of the tungsten powder. Care must be taken during the final machining not to contaminate the emitter smearing the pores with the metal particles from the cutting tool. Another promising alternative is to create more regular pores by sintering tungsten wires as proposed by Ives and Falce (2006). The third and the forth requirements necessitate a careful 3D thermal design not only of the emitting part but also of the heater, supporting structure, shielding parts and so on. The last requirement calls for a careful design of the electrodes of the MIG.

Despite the progress in improving the quality of the dispenser cathodes through improved design reported by Ives and Falce (2006), as well as using novel materials and improved manufacturing technologies in practice, nonuniformity of the emission is always present and should be taken into account when CAD of the EOS is being carried out.

Completely different from the thermionic cathodes are ferroelectric cathodes (FEC) (Hayashi, Flechtner, and Hotta 2002). In FEC the charge separation and emission are achieved by rapid switching of the spontaneous, ferroelectric polarization. Polarization switching can be induced by applying an electric field, mechanical pressure or thermal heating by laser radiation. Emitted current densities are of the order of 100 $\mathrm{A\,cm^{-2}}$ and pulse lengths are shorter than the excitation pulses. There are many advantages of using a ferroelectric cathode, such as room temperature operation, control of the emission by an external trigger pulse and, most importantly, high-electron current emission. Several applications of such emitters in MIGs for gyrotrons have been reported. Here however we are interested mainly in cathodes operating in powerful gyrotrons generating in the CW regime and will not discuss the latter class of cathodes.

A comprehensive review of the fundamental physics and technology of different emitters of electrons can be found in (Kuznetsov 1997, Yamamoto 2006).

# 4 Sources of emission nonuniformity and velocity spreads

A comprehensive discussion of the beam quality parameters can be found in (Tsimring 2007), where the main sources of the velocity and energy spread are analyzed (see Part II, Chap. 10.8.5 in this monograph) and their influence on the gyrotron performance are evaluated. It is emphasized that even a small energy spread $\Delta E/E \ll 1/N$ (where $N$ is the number of cyclotron rotations) can have considerable adverse effect on gyrotron operation. As main sources of energy and velocity spread the following factors are listed: (i) spread of initial electron velocities; (ii) roughness of an emitting surface; (iii) nonuniform distribution of electric and magnetic field determined by the geometry of electrodes and magnets; (iv) nonuniform distribution of an emission current on the cathode; (v) space-charge field in the beam; (vi) convective instabilities in the beam; (vii) global instabilities in the beam. Five out of these seven factors are related to the emission of the electrons from the cathode. All these demonstrate clearly the importance of the physical phenomena that take place on and near the emitting surface and necessitate the use of an adequate emission model which takes them into account.

One of the sources of the emission spread is the cathode work function distribution (WFD). A recent study by Miram, Ives, Read, Wilcox, Cattelino, and Stockwell (2004) of various oxide-coated and dispenser thermionic cathodes has shown that the effects of WFD are significant

throughout the entire temperature limited (TL) emission region and cannot accurately be represented by a constant value or a narrow WFD.

One of the causes of the nonuniformity is surface roughness (micro relief). The emitting surface of the cathode of a MIG for gyrotrons must be machined carefully in order to ensure smoothness on a micron level scale (Ives and Falce 2006). In practice, however, the machining tools are never perfect and always leave some marks on the cathode surface. For example, the profilimetry measurements by Jensen, Law, and Jordan (2006) show that the usual treatment of the cathode (which is accompanied by a slight wobble about the axis and ellipticity of the cathode cross section) produces parallel micron-scale ridges along the surface. As a result, for the conical cathodes that are usually used in gyrotrons, an angular variation of the field enhancement factor is observed. This means that each ridge (or more generally each area with enhanced field) provides additional emission current on an otherwise uniform cathode. The model shows that large-scale angular variations in the emission current (when the currents in adjacent quadrants differ, for example, by a factor of 2) can be explained by the angular variation of the field enhancement factor. In other words, the dependence of the field enhancement parameter $\beta(\theta)$ on the azimuthal angle $\theta$ is transformed into an azimuthal variation of the current $I_1(\theta) = I_0[1 + \alpha(\theta)]$, where $I_0$ is the current on a smooth cathode, and $\alpha$ is the local increase in the current density due to the presence of parallel ridges with mean separation $\Delta$ and width $\delta$ given by

$$\alpha = \frac{\delta}{\Delta}\left[\frac{J(F,T)}{J(F_0,T)} - 1\right].$$

Here, $F_0$ is the macroscopic electric field, and $F = \beta F_0$ is the locally enhanced field on the ridges. For the specific case when the field enhancement is caused by off-axis rotation and an ellipsoidal cross-section of the cathode cone its azimuthal dependence is

$$\beta(\theta) \approx \beta_0 + \beta_1 \cos(\theta + \varphi_1) + \beta_2 \cos(2\theta + \varphi_2), \tag{22}$$

where the second term corresponds to off axis rotation and the third one to the elliptical characteristics, respectively. The constants in the above equation depend on the shape of the ridges. Typical values considered in (Miram, Ives, Read, Wilcox, Cattelino, and Stockwell 2004) are $\beta_0 = 76.0$, $\beta_1 = 17.6$, $\beta_2 = -13.6$, $\varphi_1 = 0.9°$, and $\varphi_2 = -45.67°$. For this particular example, when $\beta$ is of the order of 60 and $\alpha$ is on the order of unity, the azimuthal variation is 2:1.

Assuming that the work function distribution is Gaussian with a mean value $\phi_0$ and standard deviation $\sigma$, the current density is given by (Anderson, Korbly, Temkin, Shapiro, Felch, and Cauffman 2002, Anderson, Temkin, and Shapiro 2005)

$$\begin{aligned} J =& \frac{\kappa V^{3/2}}{2}\left[1 + \operatorname{erf}\left(\frac{\phi_\mathrm{T} - \phi_0}{\sigma\sqrt{2}}\right)\right] \\ &+ A_\mathrm{RLD} T^2 \left[1 - \operatorname{erf}\left(\frac{\phi_\mathrm{T} - \phi_0 + e\sigma^2/k_\mathrm{B}T}{\sigma\sqrt{2}}\right)\right] \exp\left[-\frac{e}{k_\mathrm{B}T}\left(\phi_0 - \sqrt{\frac{eE}{4\pi\varepsilon_0}} - \frac{e\sigma^2}{2k_\mathrm{B}T}\right)\right], \end{aligned} \tag{23}$$

where $\kappa$ is is the perveance of the beam (dependent on cathode geometry). $E$ is the electric field which contributes to the Schottky effect. The transitional work function $\phi_\mathrm{T}$ is the work function at the threshold voltage where the space-charge limited current is equal to the temperature-limited current.

In the framework of this model a distinction is made between the global and local work function spreads. Such approach is justified by the well-known observation showing that small areas of the cathode (of the order of 500 $\mu m^2$) may have an internal variation of the work function. This variation occurring on a microscopic area is denoted as a "local." At the same time, different regions of the emitter, separated by distances of the order of several centimeters, may have different local mean values of the work function. Therefore, the latter variation is referred to as a "global" spread in work function. Statistically, when these two spreads are uncorrelated the total spread is given by

$$\sigma^2_{\text{total}} = \sigma^2_{\text{global}} + \sigma^2_{\text{local}}. \tag{24}$$

The local spread can be caused by distribution of the barium coverage, which on turn depends on the pore sizes. Experimentally the local spread can be determined measuring the current over small locations of the cathode. Alternatively, one can first determine the global spread and then calculate the local spread from the above relation.

In (Anderson, Temkin, and Shapiro 2005) is stated that "Emission nonuniformity due to a temperature distribution for a gyrotron cathode has been shown, both from theory and direct measurement (Anderson, Korbly, Temkin, Shapiro, Felch, and Cauffman 2002), to be small compared to nonuniformities caused by a spread in the cathode's work function for most MIGs."

The effects of the roughness of the cathode surface on the emittance of an electron beam in a gyrotron gun were investigated by (Borie and Horcher 1997).

The model of a single bump on the cathode surface is shown schematically in Fig. 8. In a

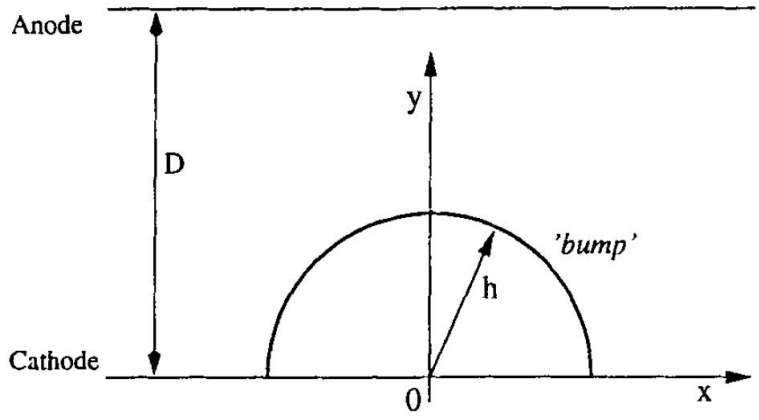


Figure 8: Bump on the emitting surface modelled by a hemisphere.

MIG for gyrotrons the surface roughness is $h \approx 5$–$20$ μm and $h/D \ll 1$. The electric field for this geometry is calculated using a conformal mapping with the following transformation:

$$u + iv = z + \frac{h^2}{z}, \tag{25}$$

where where $z = x + iy$. This yields

$$u = x\left(1 + \frac{h^2}{x^2 + y^2}\right),$$
$$v = y\left(1 - \frac{h^2}{x^2 + y^2}\right). \tag{26}$$

For this transformation, the lower electrode with the bump corresponds to $v = 0$. The electric field components accordingly are

$$E_x = -2E_0 \frac{xyh^2}{(x^2 + y^2)^2},$$
$$E_y = -E_0\left[1 - \frac{h^2(x^2 - y^2)}{(x^2 + y^2)^2}\right]. \tag{27}$$

where $E_0$ is the unperturbed electric field in a parallel plate capacitor. Electric field lines and equipotential surfaces near the bump are shown in Fig. 9.

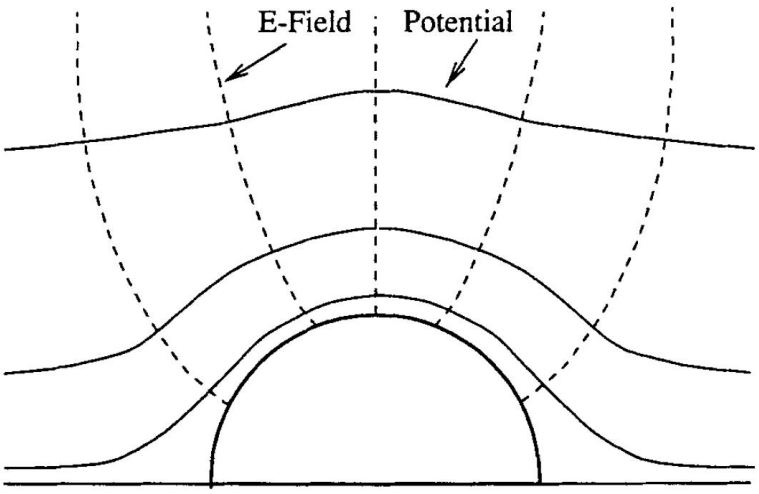


Figure 9: Electric field lines and equipotential surfaces near the bump.

The starting points of the trajectories ($x_0$ and $y_0$) are found from the conformal mapping, by varying $u_0$ with $v_0 = 0$. All particles start with zero initial velocities. The magnitude of the electric field $E_0$ was varied from 1 $\mathrm{kV\,mm^{-1}}$ to 5 $\mathrm{kV\,mm^{-1}}$; that region corresponds to values of the field near the emitter in a typical MIG. The height of the bump was varied from 0.002 mm to 0.02 mm, also corresponding to physically realistic values. The size of the computational region was adjusted to correspond approximately to the size of an emitter cell in a calculation with BFCPIC/BFCRAY. When computing averages, the contributions of the electrons starting from a point on the bump are weighted with the ratio of the area of the bump to that of the entire emitting surface. The data obtained from ray-tracing experiments indicate that the

spread in emission angle resulting from a hemispherical bump having a height $h$ between 2 μm and 20 μm is somewhere between 2° and 20°. The influence of the bump is most pronounced in the first ten percent of the emitting cell. A reasonable model for the emitter surface in a gyrotron gun would be randomly distributed surface irregularities with heights between 5 μm and 20 μm. Another conclusion made in (Borie and Horcher 1997) is that including a randomly distributed initial pitch angle varying from 6° and 20° with respect to the perpendicular should approximately simulate the spread in initial angle due to surface roughness. In (Krasilnikov 2006) the configuration of the two-dimensional bump (Fig. 10) is given by

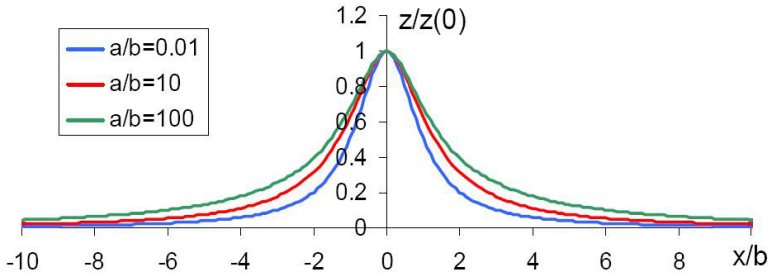


Figure 10: Model of a single bump. The upper curve corresponds to $a/b = 100$.

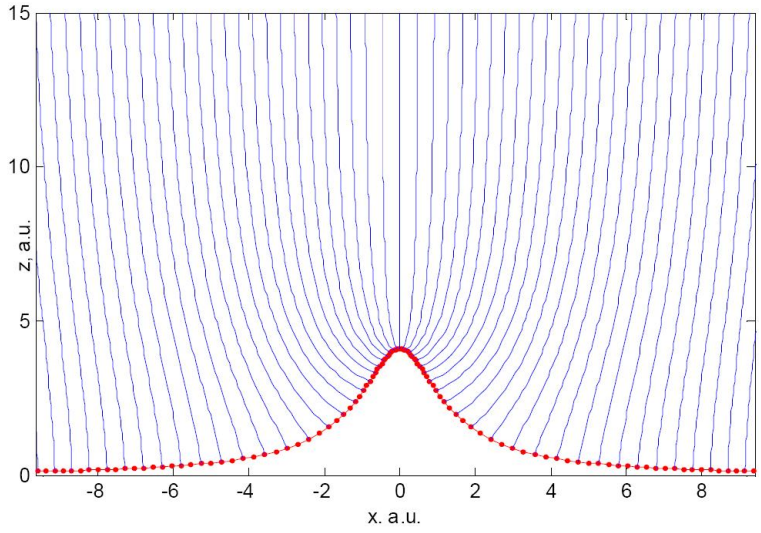


Figure 11: Electric field lines near the aforementioned bump.

$$\frac{z}{b} = \sqrt{1 + \frac{a^2}{b^2 + x^2}} - 1, \tag{28}$$

where the parameters $a$ and $b$ are constants depending on the depth and the width of the roughness, respectively. The conformal transformation which maps the field of a plane capacitor onto the field of the surface (28) is

$$u + iv = \sqrt{[x + i(y + b)]^2 + a^2} - ib. \tag{29}$$

Using this mapping, the electric field can be obtained in the following form:

$$E_x + iE_y = \frac{-iE_0[x - i(y + b)]}{\sqrt{[x - i(y + b)]^2 + a^2}}. \tag{30}$$

The electric field lines of the single bump (28) are shown in Fig. 11.

# 5 Influence of the emission nonuniformity and velocity spread on the gyrotron performance and the necessity to take into account these factors in numerical simulations

It is generally accepted that the beam quality parameters and eventually the overall gyrotron performance depend critically on the nonuniformity of the emission. Some of the known and experimentally observed adverse effects that are spurred by the nonuniformity of the current extracted from the emitting part of the cathode in the gyrotrons are: mode competition, mode hopping, efficiency degradation, and severe local heating in the collector region (Anderson, Korbly, Temkin, Shapiro, Felch, and Cauffman 2002; Jensen, Feldman, and O'Shea 2004; Anderson, Temkin, and Shapiro 2005).

A quasilinear theory of mode interaction in gyrotrons with azimuthally inhomogeneous electron emission was developed by Nusinovich and Botton (2001). The results of this theory predict that at low currents the inhomogeneity may cause excitation of additional modes at the frequency of the operating one. At higher currents, one can observe the onset of phase-locked triplets with an equidistant frequency spectrum. As the inhomogeneity increases, this enhances the beating effects in such triplets, e.g., the mode amplitudes exhibit some oscillations whose period is inversely proportional to their frequency separation and whose modulation increases with the inhomogeneity in the beam current. The analysis performed in (Nusinovich and Botton 2001) shows that the inhomogeneity causes additional coupling between modes which are orthogonal in the absence of the inhomogeneity. In gyrotrons with a quasi-equidistant spectrum of mode frequencies this causes the formation of stable triplets, in which the ratio of intensities of the satellites to the intensity of the central mode increases with the emission inhomogeneity. This additional coupling also causes fast oscillations in the mode amplitudes, which are especially well seen for those modes whose amplitudes are small.

Numerical simulations (Nusinovich, Vlasov, Botton, Antonsen, Cauffman, and Felch, 2001) with the MAGY code demonstrate that the azimuthal inhomogeneity of the emission may cause the appearance of pulsating satellites in the vicinity of a high-order operating mode. In the case of typical nonuniformity of the emission and typical dependence of the velocity spread on the beam current, the efficiency can be 2%–3% lower than in gyrotrons with ideally uniform emission.

The influence of the azimuthal nonuniformity of the emission on the beam quality parameters has been studied experimentally by Glyavin, Goldenberg, Kuftin, Lygin, Postnikova, and Zapevalov (1999). The method used is based on the analysis of the transition region between space charge limited emission and temperature limited emission on the measured current–voltage ($I$–$V$) characteristic of the cathode. It is assumed that different regions of the emitter can operate in different regimes and that with increasing applied voltage the total area of regions emitting in the space charge limited regime grows while that of temperature limited extraction shrinks. The transition voltage for each elementary section of the cathode area depends on its emitting properties, and the more homogeneous the cathode is in terms of emission, the narrower the transition zone. Density distribution function $F(J)$ is evaluated as the second derivative of the $I$–$V$ characteristic of the cathode

$$F(J) = -\frac{1}{p^2}\frac{d^2 I}{dx^2}, \tag{31}$$

where $p$ is the perveance and $x = V^{3/2}$.

The results of the experiments show significant deterioration of the gyrotron efficiency with increasing inhomogeneity of the emission (Fig. 12).

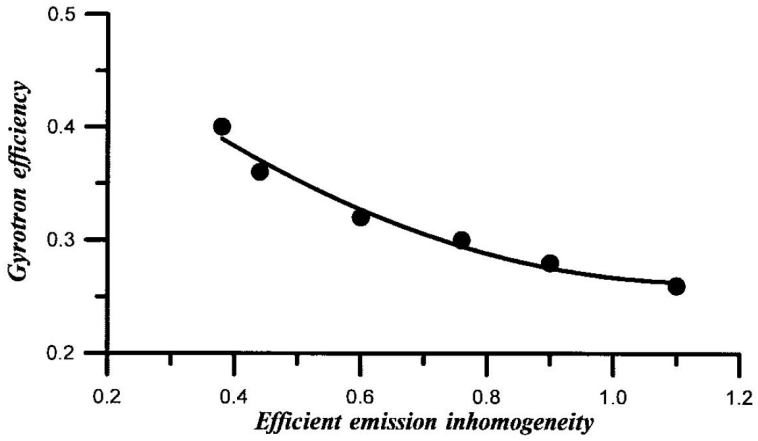


Figure 12: Dependence of the efficiency on the emission nonuniformity measured by the parameter $\sigma$ which is equal to the standard deviation of the normal distribution $F(J) = (1/\sqrt{2\pi}\sigma)\exp[-(1-x)^2/2\sigma^2]$ that approximates the measured one [from (Glyavin, Goldenberg, Kuftin, Lygin, Postnikova, and Zapevalov 1999)].

The results of experimental and numerical studies in (Louksha, Piosczyk, Sominski, Thumm, and Samsonov 2006) show that the observed increase of the low-frequency oscillations in the case of inhomogeneous emission is due to the corresponding increase of the velocity spread in the electron beam.

The evolution of an electron beam with azimuthal density nonuniformity in a cylindrical beam tunnel has been studied by Pagonakis and Vomvoridis (2004). It has been found that the azimuthal nonuniformity causes effects clearly associated with $\mathbf{E} \times \mathbf{B}$-drifts. The numerical results show, however, that these effects are too small to affect the performance of gyrotrons.

# 6 Emission models implemented in the ray tracing and PIC simulation tools

## 6.1 Emission model of the EGUN code

The well-known *SLAC Electron Trajectory Program* (EGUN) (Herrmannsfeldt 1988) is one of the best-known codes for numerical simulation of electron guns, including space charge, Child–Langmuir and Fowler–Nordheim starting routines and 3D relativistic trajectory calculation in 2D rectangular or axially symmetric electric and magnetic fields.

The electric field and potential are held to zero on the starting surface, and the iteration proceeds. The current filaments act on one another in a reasonable approximation, and magnetic focusing is incorporated taking into account the azimuthal component of the self magnetic field, which is superimposed on the external magnetic field. It should be mentioned that such an approach is realized in the most of the known codes described below, but will not be repeated again. To simulate initial velocities effects in the beam, each filament is subdivided into rays of varying strength and they are emitted at specified angles from the normal to the starting surface. These filaments are quickly curved back toward the direction of the normal, as no crossing of the filaments is allowed in the calculation.

There are several possibilities to specify the emission model of the cathode:

(i) "GENERAL" cathode in which electrons are started assuming that Child's law holds near a surface designated as the cathode. This surface can be of any arbitrary shape and may include holes and shadow grids.

(ii) "SPHERE" for a spherical cathode (cylindrical in rectangular coordinates) in which the electrons are assumed to be emitted at right angles to the surface defined by a radius of curvature and a radial limit. Child's law for space-charge limited current is again used.

(iii) "CARDS" in which the specific starting conditions for each ray are specified.

(iv) "GENCARD" which combines the versatility of "CARDS" with the assumptions of Child's law from "GENERAL." This is especially useful for cases involving a very nonuniform current emission.

In order to simulate the effect of thermal velocities, each ray can be divided into two or more rays with any desired fraction of the current in each ray such that the total is 100%. The initial angle can then be varied differently for the different rays to simulate thermal noise on the beam.

The program accepts the beam temperature in Kelvin and calculates a radial increment to be added and subtracted from particles that start from the initial coordinates of each "ideal" particle; before adding the thermal energy (Herrmannsfeldt 1994). There are three models, using two, three, and five particles, respectively, for each initial particle. The two-particle model is the most satisfactory because it includes a random number generator to give the statistical sense to the thermal processes (Herrmannsfeldt 1994).

It is important to note that the three methods for initiating a space-charge limited flow all include a Busch's theorem calculation to account for the magnetic flux through the cathode.

## 6.2 Emission model of the CIELAS2 code

The emission model for a thermionic cathode implemented in the CIELAS2 code (Edgcombe 1995) can treat both space charge limited and temperature limited emission. The density of

emitted current is set by the choice of the temperature and thermionic properties of the cathode. The starting point for each trajectory is a small fraction of a mesh, spacing from the cathode, in the region where the potential can be estimated using thermal velocity theory. The charge density deposited up to a short distance beyond the minimum potential is that appropriate to thermally-distributed velocities. The resulting estimates of the electric field at the cathode surface are expected to be more accurate than those found by programs which start trajectories at a greater distance from the cathode (Edgcombe 1995). The number of emission points and number of trajectories started at each point can be varied to provide 240 trajectories or more. At any point, rays can be started with chosen numbers of initial directions, both in angle to the normal and in azimuth. For any point and direction, rays can be emitted with more than one value of the initial energy. This capability has allowed the velocity spread arising from these initial variations to be compared with that due to other causes. The magnitudes of currents are assigned by use of a simple cosine model for the distribution of emitted current density.

The results of numerical experiments indicate that initial velocity spreads at the cathode appear to be less important in determining the final velocity spread than the effect of nonuniformity of the electric field over the emitter surface, at least in the limit of temperature limited emission.

## 6.3 Emission model of the BFCPIC, BFCRAY and ESRAY codes

The emission model realized in the BFCPIC and BFCRAY codes can be described as follows (Borie and Horcher 1997): (i) new particles are emitted from each emitter cell (randomly located within each cell) at each time (or iteration) step. (ii) The charge on each macroparticle is adjusted to maintain the given total current and is given by $Q = I\Delta t/n_{\rm new}$, where the number of new emitted particles is user defined. If uniform emission over the emitter is assumed, then the number of particles emitted at each time step should be equal to the number of grid cells on the emitter, or an integral multiple thereof. (iii) All emitted particles have the appropriate physical charge to mass ratio. A typical value of $Q$ for a macroparticle is about $10^{-11}$ C, corresponding to about $10^8$ electrons.

In the initial version of this model the kinetic energy of the emitted particles is set equal to zero, since the kinetic energy of the emitted particles is typically much smaller than the energy acquired in crossing one cell near the emitter. In order to ensure that the space charge distribution is modelled by a reasonably smooth function, the location of the newly emitted particles is varied randomly, but uniformly over the emitter surface. The fields must be correctly interpolated to the actual particle position and a sufficiently large number of particles must be emitted at each iteration step.

The basic emission model described above has been modified in order to take into account the initial velocity spread modelled by an effective scatterer in initial pitch angle. As a starting point, one assumes a smooth emitter surface that emits particles perpendicular to it. At a fixed distance from the emitter (almost always equal to 0.01×cell height), the additional spread in pitch angle is included (see Fig. 13). The initial pitch angles are denoted by RTHET (the angle in the $X1$–$X2$-plane), and RPHI (the angle perpendicular to the $X1$–$X2$-plane, i.e., the azimuthal angle). The starting point (RX) along the emitter is determined randomly. Then the electrostatic potential $\phi$ at point P is computed from the potential differences between the cell corners. The magnitude of the initial velocity is then determined from the energy conservation law, $mv^2/2 = e\phi$.

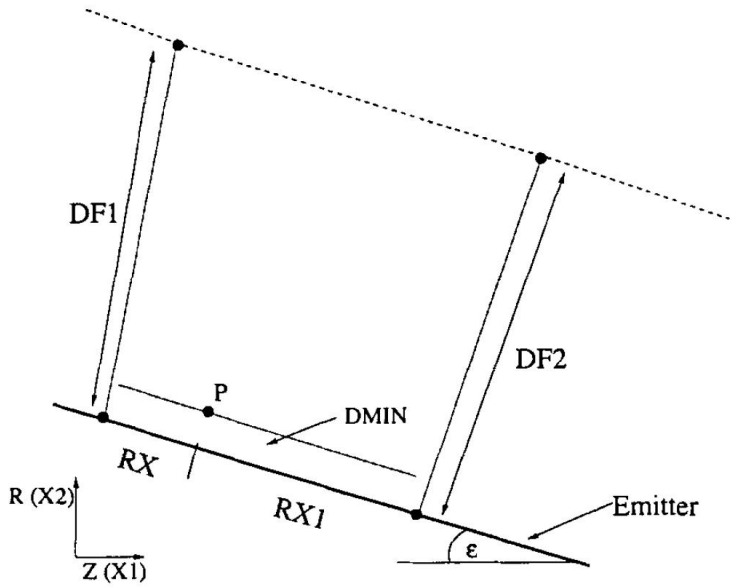


Figure 13: Emitting cell on the cathode [from (Borie and Horcher 1997)].

The slope $\varepsilon$ of the cathode determines the components $v_{x1}$ and $v_{x2}$ of the initial velocity (see Fig. 14) in the directions of $X1$ and $X2$. The additional angle RTHET is added to or subtracted from in order to simulate the spread in pitch angle resulting from surface roughness. An azimuthal velocity component $VX3$ pointing into or out of the page and is determined by the angle RPHI. It is possible to vary RTHET and RPHI independently between user-defined limits.

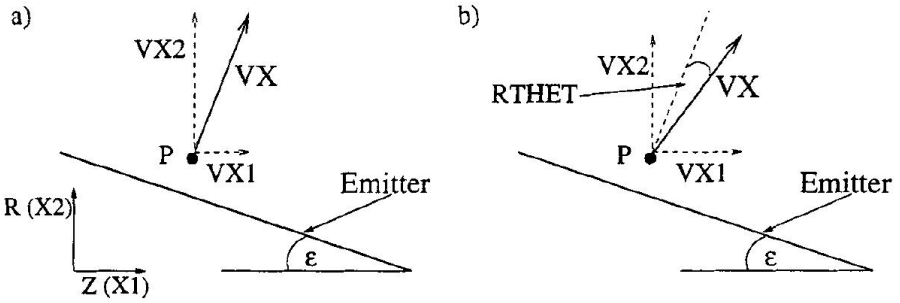


Figure 14: (a) Emission without scatter in pitch factor, and (b) with scatter (RHTET is added to the emission angle) [from (Borie and Horcher 1997)].

In the case of space charge limited emission each emission cell is considered as a planar diode and the extracted current density $J_{\mathrm{CL}}$ is calculated from Child's law (Borie, Illy, and Westermann 1997). More specifically, assuming that the distances $d_1$ and $d_2$ (see Fig. 15) are

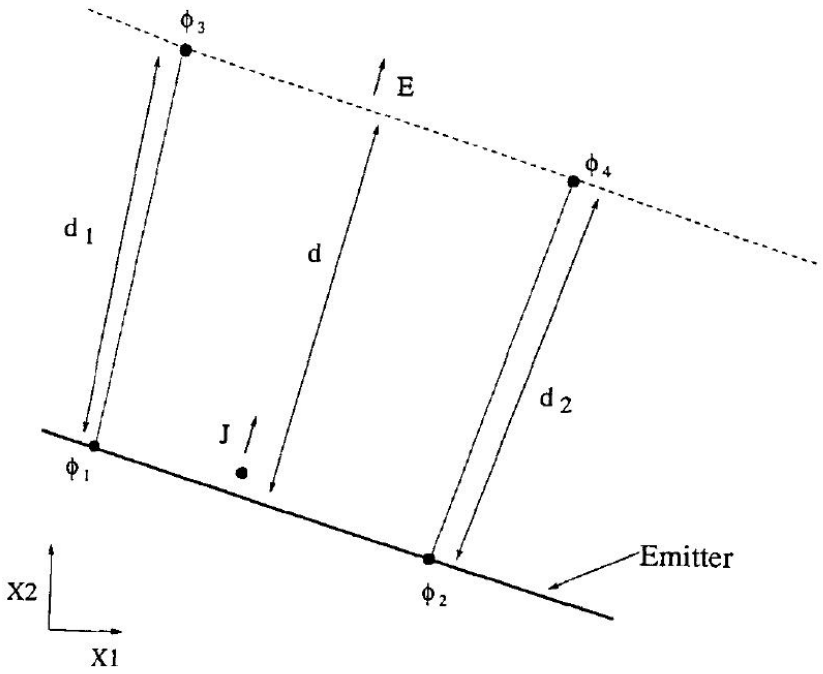


Figure 15: Emission cell for calculation of the extracted current from Child's law.

small and averaging the current densities for the left and right edges one gets

$$J_{\mathrm{CL}} = \frac{4}{9}\varepsilon_0\sqrt{\frac{2e}{m}}\frac{1}{2}\left[\frac{(\phi_3-\phi_1)^{3/2}}{d_1^2}+\frac{(\phi_4-\phi_2)^{3/2}}{d_2^2}\right]. \tag{32}$$

Once the current density is determined in each cell, the emitted charge is determined by

$$Q_{\mathrm{emit}} = J_{\mathrm{CL}} A \Delta t, \tag{33}$$

where $A$ is the emitting area and $\Delta t$ is the time step. In practice $J_{\mathrm{CL}}$ is calculated in this way only in the PIC version (BFCPIC), using a shorter calculation region without the beam tunnel. The resulting current density in each cell could be read in for ray tracing.

## 6.4 Emission model of the EPOS-V code

It was already mentioned that the initial velocity spread is due to the presence of inhomogeneous axially-symmetric fields at the cathode, determined by the geometry of electrodes and of the magnetic system, to the thermal velocity spread and to the roughness of the emitting surface of the cathode. Taking into account the specific formation of the oscillatory velocities in a MIG, the developers of the EPOS-V code (Lygin 1995) proposed to replace the joint influence of these factors by an appropriately chosen azimuthal initial velocity, $v_{\varphi 0}$. The initial velocities in other directions are assumed to be zero, since they affect the velocity distribution only slightly.

In the numerical simulation the electron beam is replaced by a set of current tubes, each of which is divided into several velocity groups with various values of the current $dI$ and the

azimuthal velocity, $v_{\varphi 0}$. The latter should, in principle, be calculated from the initial velocity distribution, $dI/dv_{\varphi 0}$. But since this distribution is not known, it is approximated by a normal one. The parameters of the normal (approximating) distribution are chosen in such a way for $I \approx 0$ as to coincide with the experimentally measured one.

A version of the EPOS-V code (Lygin, Manuilov, and Tsimring 1999) which is based on a non-stationary physical model that can account for the reflected electrons uses the following procedure to simulate the emission.

At each instant of time $t_i = i\Delta\tau$ $(i = 1, 2, \ldots)$ $N_z N_v$ particles start from the emitter ($N_v$ is the number of the velocity groups with different $v_{\varphi 0}$ and corresponding values of particle charge calculated according to the initial velocity distribution $dI/dv_{\varphi 0}$ on the cathode, $N_z$ is the number of elementary rings with areas $S_k$). The charge of the starting particle is obtained as $Jdt\, S_k f(v_{\varphi 0})$.

## 6.5 Emission model of the GPT and PARMELA codes

The initial particle distribution in the General Particle Tracker (GPT) code (van der Geer 2001) is essential for correct simulation results because it defines the boundary conditions for the ODE solver. Creating this 6D phase-space consisting of all 3D position and 3D momentum coordinates of the initial particles can be quite challenging. GPT, just like PARMELA, has the capability to read the initial particle distribution from a file. As a result both programs are capable of starting any possible distribution.

PARMELA (Young 1996) uses one routine that can be used to start the electron bunches. This distribution is based on the Courant-Snyder parameters without detailed control over the underlying distributions. This is very inflexible because for example a hollow beam, a cosine or linear particle density distribution and a square beam must all be created externally.

## 6.6 Emission model of the GUN-EBT and GUN-MIG/CUSP codes

Although the emitter in a MIG for gyrotrons most often operates in a temperature limited mode, in the GUN-MIG/CUSP code (Sabchevski, Mladenov, and Idehara 1999) Langmuir's theory is included in the physical model in order to extend the applicability of the code to cases where the whole area of cathode or some regions of it are operating in a space charge limited regime. According to this approach, it is assumed that the region near the emitter can be divided into a number of small virtual diodes in which the current is governed by the potential distribution and initial velocities of the thermoelectrons. It is also assumed that in each virtual diode Langmuir's theory holds and the technique described in (Sabchevski, Mladenov, Titov, and Barbarich 1996) is applied for computation of the extracted currents.

It is based on the fact that the initial velocities of electrons in the beam are determined by the temperature of the emitter and usually correspond to energies less than 1 eV. As a result, the space-charge density in the vicinity of the cathode is high and significantly affects the potential distribution. Moreover, usually a space-charge cloud forms which produces a potential minimum in the vicinity of the emitter. A fraction of the emitted electrons does not have sufficient energy to surmount the potential barrier and returns to the cathode. It is important to note that in reality various cathode regions can function under different operating conditions. For instance, if there is no potential minimum in front of a particular cathode area all emitted electrons will be extracted by the accelerating field and will take part in the beam formation. This regime

is called the saturation or temperature limited mode of operation. At the same time, other cathode regions in front of which emitted electrons face a retarding electric field will work in the space charge limited mode. In the former case the current density is given by

$$J = J_{\mathrm{sat}}, \tag{34}$$

while in the latter

$$J = J_{\mathrm{sat}} \exp(\phi_{\mathrm{min}}/k_{\mathrm{B}}T), \tag{35}$$

where $J_{\mathrm{sat}}$ is is the temperature limited current density (also called "saturated current density") calculated from the Richardson–Dushman equation and $\phi_{\mathrm{min}}$ is the potential minimum.

In order to take into account both the initial thermal velocities of the electrons leaving the cathode and variations of the potential near the emitter, the cathode surface is divided into a number of small annular regions. The extracted current density in each annular region is calculated by considering it as a small planar diode and by applying Langmuir's theory. Langmuir's solution for a planar diode relates the dimensionless potential

$$\eta = \frac{e}{k_{\mathrm{B}}T}(\phi - \phi_{\mathrm{min}}), \tag{36}$$

and the dimensionless distance

$$\zeta = \chi(z - z_{\mathrm{min}}), \tag{37}$$

where $z_{\mathrm{min}}$ is the distance between the potential minimum and the emitting surface, $\chi = cT^{-3/4}J^{1/2}$, and $c$ is a constant. The dependence between $\eta$ and $\zeta$ is available in tabular form as well as in the form of approximations [$\eta = F_1(\zeta)$ and $\zeta = F_2(\eta)$], adapted to represent the tabular data with the required accuracy.

In calculations there are three known quantities for each elementary diode, namely: cathode temperature, anode potential $\phi_{\mathrm{a}}$ and anode-to-cathode distance $d_{\mathrm{a}}$. In order to obtain the extracted current density $J_{\mathrm{a}}$, an iterative procedure is used to solve the transcendental equation

$$\phi(J_{\mathrm{a}}) - \phi_{\mathrm{a}} = 0, \tag{38}$$

taking advantage of the following relations:

$$\phi_{\mathrm{min}} = -\frac{k_{\mathrm{B}}T}{e}\ln(J/J_{\mathrm{a}}), \tag{39}$$

$$\eta_{\mathrm{c}} = -e\phi_{\mathrm{min}}/k_{\mathrm{B}}T, \tag{40}$$

$$\zeta_{\mathrm{c}} = F_2(\eta_{\mathrm{c}}), \tag{41}$$

$$\zeta_{\mathrm{a}} = \zeta_{\mathrm{c}} + \chi d_{\mathrm{a}}, \tag{42}$$

$$\phi(J_{\mathrm{a}}) = (k_{\mathrm{B}}T/e)(\eta_{\mathrm{a}} - \eta_{\mathrm{c}}). \tag{43}$$

Using the technique described above, the current density as well as the location and depth of the potential minimum for each cathode region can be calculated. The entire area of the boundary-value problem can be divided in two partially overlapping regions. The first one is the region between the cathodes and the anodes of the elementary diodes. The second region begins at the potential minimum and extends to the end of the area. Thus, the potential minimum is used as a boundary condition for the solution of Poisson's equation in the second region in order to obtain a self consistent solution.

## 6.7 Emission model of the MICHELLE code

MICHELLE 3D (Petillo, Eppley, Panagos, Blanchard, Nelson, Dionne, DeFord, Held, Chernyakova, Krueger, Humphries, McClure, Mondelli, Burdette, Cattelino, True, Nguyen, and Levush 2002) is a finite-element gun and collector modelling code developed by that incorporates a steady-state Particle-In-Cell (PIC) algorithm with conformal structured or unstructured mesh elements. It is a full three-dimensional code that includes relativistic self-fields calculations.

There are three basic emission models implemented in the MICHELLE code, namely: (i) temperature limited emission, (ii) space charge limited emission, and (iii) secondary electron emission. The first one assumes that the extracted current density is governed by the Richardson–Dushman equation.

The model of space-charge limited emission realized in MICHELLE exploits the Child–Langmuir law for a planar diode but with a correcting coefficient G, i.e.,

$$J = \frac{4}{9}\varepsilon_0\sqrt{2\frac{e}{m}}\frac{V^{3/2}}{s^2}G. \tag{44}$$

Here $s$ is the inter-electrode distance of the diode and

$$G = G_T G_R G_C, \tag{45}$$

where $G_T$ is a temperature correction factor, $G_R$ is a correction factor for relativistic diodes, and $G_C$ is a correction factor that takes into account the departure of the planar diode from the real geometrical configuration (spherical, cylindrical, conical or toroidal).

According to pioneering works of Langmuir, the temperature correction for the low-voltage region close to the emitting surface can be approximated by

$$G_T \cong 1 + 0.02468(T/V)^{1/2} - 0.00197(T/V)^{3/4}. \tag{46}$$

It should be noted however that this approximation is inaccurate for voltage levels below 10 V.

The relativistic correction factor is calculated from the following series expansion

$$G_R = 1 - 0.107u + 0.02418u^2 - 0.007u^3 + 0.002307u^4 - 0.0008229u^5 + \cdots, \tag{47}$$

where $u = eV/m_0c^2 = \gamma - 1$.

The geometrical correction factor $G_C$ for a planar diode inferred from the Langmuir–Blodget spherical diode analysis will be denoted by $G_S$. It may be expressed in terms of the normalized distance parameters, $s_\pm = \pm(r - r_\mathrm{c})$, as

$$G_{S_\pm} = (s_\pm/r\alpha_\pm)^2 = \left\{(s_\pm/r_\mathrm{c})\left[(1 \pm s_\pm/r_\mathrm{c})\alpha_\pm(u_\pm)\right]\right\}^2, \tag{48}$$

where $r_\mathrm{c}$ is the cathode spherical radius of curvature, $u_\pm = \pm\ln(1 \pm s_\pm/r_\mathrm{c})$. Here the parameter $\alpha$ is calculated from the series expansion

$$\alpha_\pm = u_\pm \mp 0.3u_\pm^2 + 0.075u_\pm^3 \mp 0.01432u_\pm^4 + 0.00216u_\pm^5 \mp 0.00035u_\pm^6.$$

In the above equations the plus and minus signs correspond to $r \geqslant r_\mathrm{c}$ and $r \leqslant r_\mathrm{c}$, respectively. As shown in Fig. 16, the Child's law calculations are applied and averaged at a locus of equally spaced points distributed over a few mesh cells. In such a way the interpolated potentials are

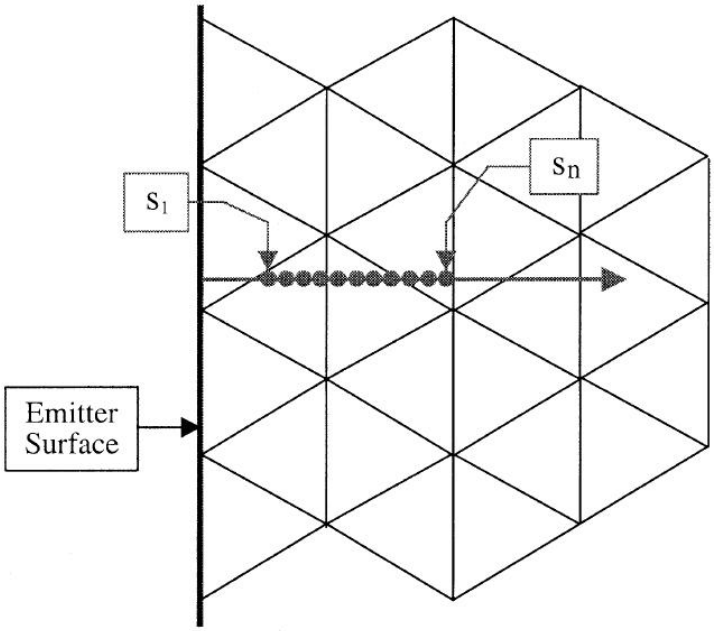


Figure 16: Integration path for the Child–Langmuir law along a surface normal direction on an arbitrary mesh cross section [from (Petillo *et al.* 2002)].

smoothed. Evaluating the current density along a distribution of points one can calculate an averaged value

$$J = \frac{4}{9}\varepsilon_0 \frac{\sqrt{2e/m_0}}{N} \sum_{n=1}^{N} \frac{V_n^{3/2}}{s_n^2} \left\{ 1 + 3 \left[ \frac{(\pi/4) k_{\mathrm{B}} T}{e V_n} \right]^{1/2} \right\} G(eV_n/m_0c^2) G_C. \tag{49}$$

In the above equation the summation spans only those points that have positive interpolated potential values greater than some user-determined minimum value, $V_1$. The starting point $s_1$ is calculated from Child's law

$$s_1 \cong (A/J)^{1/2} V^{3/4}, \tag{50}$$

using the potential $V$ from the previous iteration (time step). Here $A = 2.3332 \times 10^{-6}$.

Macroparticle launch energies and directions from a thermionic surface are generated using a Maxwellian energy distribution form, modified to account for the region beyond the potential well near the emission surface where no returning particles are encountered. In spherical coordinates, the combined energy and angular distribution function, governing thermionic emission, is separable and may be expressed in normalized form by

$$f(u, \theta, \phi) du \, \sin\theta \, d\theta d\phi = f(u) g(\theta) du \, \sin\theta \, d\theta d\phi, \tag{51}$$

where $g(\theta) = \dfrac{1}{\pi} \cos\theta$, $f(u) = u e^{-u}$, and

$$N(u) = \int_0^u u e^{-u} du = 1 - e^{-u}(1 + u). \tag{52}$$

The energy of the emitted particles normalized to $u = mv^2/2k_{\rm B}T$ is calculated from

$$\bar{u}_i = \frac{(u_{i+1}^2 + 2u_{i+1} + 2)e^{-u_{i+1}} - (u_i 2 + 2u_i + 2)e^{-u_i}}{(u_{i+1} + 1)e^{-u_{i+1}} - (u_i + 1)e^{-u_i}}, \quad i = 1, 2, \ldots, N_u, \tag{53}$$

using standard distribution-based averaging. The energy values $u_i$ bound the $N_u$ energy zones of equal probability. Illustration of the particle energy partitioning for equal launch probability when $N_u = 5$ is shown in Fig. 17.

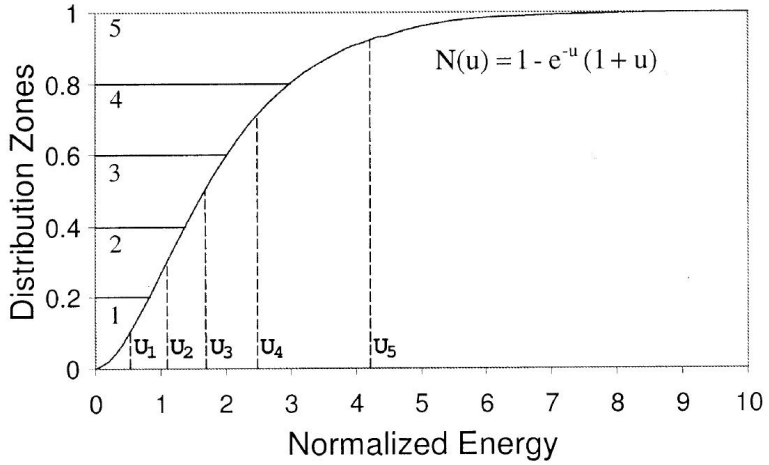


Figure 17: Illustration of average particle energies assignments for the case of five equally divided probability zones. Dashed lines correspond to the average energy centered over the indicated equal probability zones [from (Petillo *et al.* 2002)].

The corresponding angular distribution of emitted particles is isotropic about any point of emission. The angular distribution integral is

$$G(\theta) = \int_0^{\theta} g(\theta) \sin\theta \, d\theta \int_0^{2\pi} d\phi = \sin^2\theta. \tag{54}$$

The integration of $G(\pi/2)$ over the entire interval is normalized to unity. If the number of the azimuthal launch direction is $N_p$, the number of inclination angles $\theta$ is $N_i$ and the surface normal direction index $N_k$ (0 – no launch, 1 – launch), then the total number of unique launch angles is given by

$$N_i = N_p N_i + N_k. \tag{55}$$

The bounding probability fractions for each $n$th inclination cluster (see Fig. 18) are calculated from

$$\beta_n = \arcsin\left(\{[N_i + N_p(m-1)]/N_i\}^{1/2}\right), \quad m = 1, \ldots, N_i + 1. \tag{56}$$

The zone-averaged angle of inclination $\bar{\theta}_n$ for the $n$th zone is evaluated using a closed form solution

$$\bar{\theta}_n = \frac{1}{2}(\sin 2\beta_{n+1} - \sin 2\beta_n - 2\beta_{n+1}\cos 2\beta_{n+1} + 2\beta_n \cos 2\beta_n)/(\cos 2\beta_n - \cos 2\beta_{n+1}). \tag{57}$$

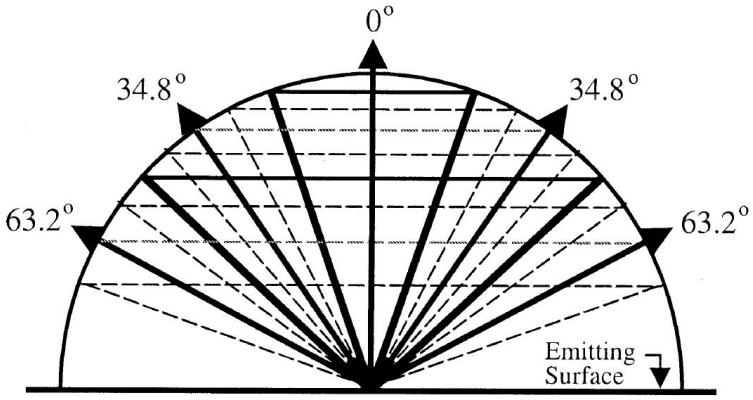


Figure 18: Cross section of discrete particle launch directions computed for a nine-particle launch case ($N_i = 2$, $N_p = 4$, $N_k = 1$, $N_t = 9$) [from (Petillo *et al.* 2002)].

The azimuthal angles of the macroparticles, emitted with equal probability are calculated from

$$\phi_m = (m-1)2\pi/N_p, \qquad m = 1, \ldots, N_p. \tag{58}$$

An example that illustrates this algorithm is shown in Fig. 18. Only five rays are visible in the cross-sectional view since four rays are located in the orthogonal plane, rotated 90° about the surface normal.

Since the secondary electron emission will be discussed elsewhere, we do not review the secondary emission model of MICHELLE in the present study. We note, however, that secondary electron emission is also being built into the ESRAY code.

## 6.8 Emission model of the BOA code

The Beam Optics Analysis (BOA) code simulates electron trajectories in 3D electromagnetic fields and geometries (Ives, Bui, Vogler, Nelson, Read, Shephard, Bauer, Datta, and Beal 2006).

The program supports several emission options, including thermionic, secondary, and injected beams. For thermionic cathodes, the user can specify cathode temperature and work function. Each emitter can operate with different parameters. According to (Ives, Bui, Vogler, Nelson, Read, Shephard, Bauer, Datta, and Beal 2006) the future versions will allow variation of work function or temperature over a cathode surface.

## 6.9 Emission model of the MAGIC code

MAGIC is a user-configurable code that solves Maxwell's equations together with the Lorentz equation of motion for particles (Goplen, Ludeking, Smithe, and Warren 1995). A variety of 2D, finite-difference electromagnetic algorithms and 3D Particle-In-Cell algorithms may be combined in problem-specific ways to provide fast, accurate, steady-state and transient calculations. MAGIC has a fully 3D counterpart called SOS. Programs exist to connect these analysis' tools to parametric and CAD input from an integrated design environment.

Macroparticles are created in the simulation either by an emission process or by entering through a boundary. They may also be populated in the simulation as an initial condition. The creation of macroparticles is inherently statistical in nature. Other options, common to all of the emission processes, control other aspects of creation. For example, an initial spacing option allows uniform, random, or weighted macroparticle placement, both transverse and normal to the emission surface.

Field emission, in which the energy required to overcome a material work function is supplied by an electric field, is described by the Fowler–Nordheim equation. In the case of thermionic emission the current density is calculated from the Richardson–Dushman equation. The beam injection model specifies a beam to be emitted from an emitting surface. It is used when the time and spatial profile of the incident current density is known, or to model a beam created outside the simulation space. It is also used in conjunction with the secondary emission calculations.

## 6.10 Emission model of the Gun3p code

Figure 19 presents the main parameters involved in the emission model of the Gun3p code

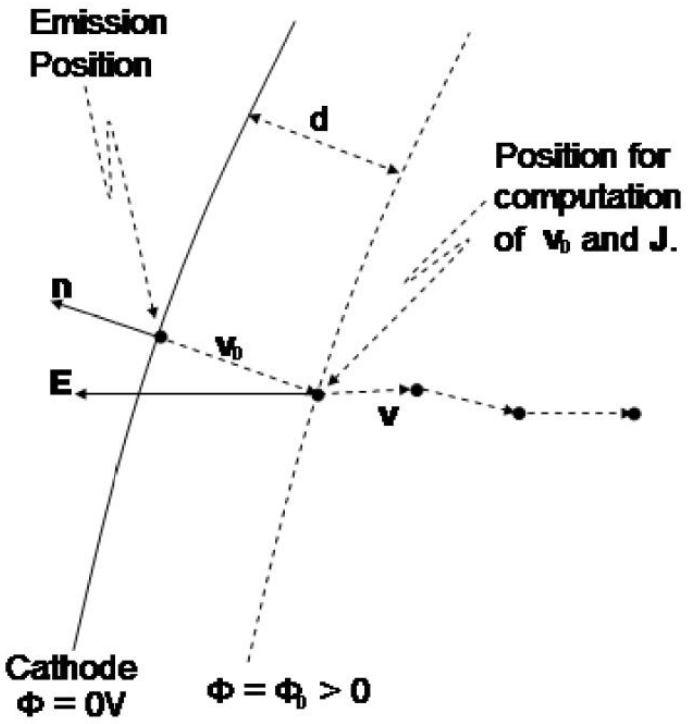


Figure 19: Emission model used in Gun3p (Prudencio *et al.* 1995).

(Prudencio, Candel, Ge, Kabel, Ko, Lee, Li, Ng, and Schussman 2008). The emission positions are assigned during initialization and do not vary through cycles. Here $\mathbf{x}_0$ indicates emission position at the cathode and $\hat{n}$ indicates the outward unit normal at $\mathbf{x}_0$. Using a user defined distance $d$ (e.g., $d = 100$ μm) from the cathode, one finds from conservation of energy that at

$\mathbf{x}_d = \mathbf{x}_0 - d\hat{n}$,

$$\frac{m_0 v_d^2}{2} = -e\phi_d, \tag{59}$$

where $m_0$ is the particle rest mass, $v_d$ is the speed of an electron at distance $d$ from the cathode, and $\phi_d$ is the electric potential at the position $\mathbf{x}_d$. Gun3P emits a particle at $\mathbf{x}_0$ with constant velocity

$$\mathbf{v}_0 = -\frac{2}{3} v_d \hat{n} \tag{60}$$

and associates to it a current density $J_{\text{cathode}}$ according to the Child–Langmuir law

$$J_{\text{cathode}} = \frac{4}{9}\varepsilon_0 \sqrt{\frac{2e}{m_0}} \frac{\phi_d^{3/2}}{d^2}.$$

Once the particle reaches $\mathbf{x}_d$, its velocity is set to

$$\mathbf{v}_d = v_d \frac{e\mathbf{E}_d}{\|e\mathbf{E}_d\|} \tag{61}$$

(with $\mathbf{E}_d = -\nabla\phi_d$) and its trajectory is computed through the relativistic Lorentz equation

$$m_0 \frac{d(\gamma \mathbf{v})}{dt} = e(\mathbf{E} + \mathbf{v} \times \mathbf{B}), \tag{62}$$

where $\gamma$ is the relativistic mass factor. The Boris algorithm (Burdsall and Langdon 1985) is used as in the BFCPIC, BFCRAY and ESRAY codes for integration of Eq. (62). Currently Gun3P does not model any thermal effects at the cathode.

# 7 General formulation of an adequate 3D emission model

The main principles that we follow in formulating a general emission model are the principle of decomposition and the principle of an equivalent diode. Accordingly, the emitting surface $\Omega_{\text{S}}$ is divided into a number $N_{\text{S}}$ of small non-overlapping regions $\Omega_{\text{S}_i}$, i.e., $\Omega_{\text{S}} = \cup \Omega_{\text{S}_i}$, $\Omega_{\text{S}_i} \cap \Omega_{\text{S}_j} = 0$, and $\text{diam}(\Omega_{\text{S}_i}) \ll 1$, where $i = 1, 2, \ldots, N_{\text{S}}$. Then each elementary region is considered as the cathode of an equivalent diode. The anode of this virtual elementary diode (usually a parallel plate diode) is either a surface obtained by translating the cathode surface in the direction of its normal or more practically an appropriate (close to the emitter) equipotential surface obtained from the current solution of the boundary-value problem for the electrostatic potential. In any case, the distance between the cathode and the anode of the equivalent diode should be much less than the transverse extent of the electrodes. Then for each elementary diode one can apply one or another of the physical models for space-charge limited or temperature limited emission discussed above. Such a formulation takes into account the fact that in practice different cathode regions can operate under different conditions (different local temperature, different local work function of the emitter, different local electric and magnetic fields and so forth). Although the elementary equivalent cathodes need to be small enough, usually their extent is covered by several elementary cells of the computational grid. This makes it possible to introduce local spatial variations of the initial conditions inside each equivalent diode in order to take into account the surface roughness, for example.

On each elementary cathode the range (distribution) of the initial energies $E_i$ corresponding to a given cathode temperature is divided into $N_E$ groups. The initial velocities of the particles belonging to the group $i$ ($i = 1, 2, \ldots, N_E$) is calculated from the relation

$$v_i = \sqrt{\frac{2E_i}{m}}. \tag{63}$$

The total current extracted from $j$th elementary cathode is

$$I_{\mathrm{tot}_i} = J_0 A_j = eA_j(n_1 v_1 + n_2 v_2 + \cdots + n_{N_E} v_{N_E}), \tag{64}$$

where $A_j$ is the emitting area, $J_0$ is the averaged current density over it and the total number of the emitted particles is

$$N_{\mathrm{tot}} = \sum_{i=1}^{N_E} n_i.$$

The number of particles in each energy group can be calculated from (Freeman 2001)

$$n_i = \frac{2N_{\mathrm{tot}}}{\sqrt{\pi}} \int_{\eta_{\min}}^{\eta_{\max}} \sqrt{\eta} e^{-\eta} d\eta, \tag{65}$$

where $\eta = E_i/E_T$ (with $E_T = k_{\mathrm{B}}T/e$) is the normalized energy and $n_i$ is rounded to the closest integer number.

Once the number of particles for each energy group $n_i$ is calculated, it must be divided into $N_\theta$ angles of emission. Denoting by $n_{ij}$ the number of particles from the $i$th energy group emitted at the $j$th emission angle, $\theta_j$, we have

$$n_i = \sum_{j=1}^{N_\theta} n_{ij}. \tag{66}$$

The method used to calculate $n_{ij}$ must correspond to the angular distribution of the emission according to Lambert's law, and, additionally, comply with the statistical characteristics of particle distribution according to the Maxwell–Boltzmann distribution. Such a method is proposed by Freeman (2001). It implies that

$$n_{ij} = n_{i1} \cos\theta_j, \tag{67}$$

where

$$n_{i1} = \frac{n_i}{\sum_{j=1}^{N_\theta} \cos\theta_j}.$$

Here $\theta_1 = 0$ and it corresponds to the emission in the direction of the normal to the emitting surface. Such a procedure complies with the well-known statistical relation (Freeman 2001), notably that the normal energy of the particles is twice its tangential value when calculated over the ensemble [see Eq. (1-15) in (Freeman 2001)].

# 8 Conclusion and outlook

In this summary the basic relations governing electron emission from thermionic cathodes used in the magnetron injection guns (MIGs) of modern gyrotrons, as well as some of the most characteristic implementations of various emission models in several ray-tracing and PIC codes have been presented. In their entirety they take into account the most important physical factors and phenomena that take place in the cathode region of the gun and which affect the beam quality parameters. Although the level of idealization is different for different codes it can be concluded that there is no simulation package that treats all emission problems of practical interest. It seems that an attempt to incorporate more emission models in the existing available codes as a part of their upgrade could involve more physics in the simulations and will make them more realistic. The realization of adequate (physics-rich) emission models in the next generation of 3D simulation tools that are under development now is mandatory. In fact, since in reality most of the distributions depart from the axial symmetry the need to treat them adequately is among the main motivations for the development of 3D codes.

It is believed that this summary contains the most important equations, formulas and methods (or references to them) that are necessary for programming implementation of the reviewed emission models. The next important task is to select the most efficient models, taking into account the necessary computational resources and the additional computational load on the codes in which such models will be incorporated.

# Acknowledgements

This study has been performed in the framework of the Contract FU06-CT-2004-00134 "Numerical investigations of selected problems associated with the development of powerful gyrotrons for fusion research" and task P3 "Development of computer codes to describe the behavior of high power gyrotrons" of the Association EURATOM-INRNE which have being pursued in a collaboration between the Institute of Electronics of the Bulgarian Academy of Sciences (IE-BAS), the Faculty of Physics of Sofia University (FP-SU), the Institute for Pulsed Power and Microwave Technology at the Forschungszentrum Karlsruhe (IHM-FZK) and the Centre de Recherches en Physique des Plasmas at École Polytechnique Fédérale de Lausanne (CRPP-EPFL). One of us (S. Sabchevski) would like to express his gratitude to the IHM-FZK for the stimulating atmosphere, nice working conditions and productive discussions during his stay in Karlsruhe under the Mobility scheme.

This work supported by the European Communities under the contract of Association between EURATOM and Forschungszentrum Karlsruhe, was carried out within the framework of the European Fusion Development Agreement. The views and opinions expressed herein do not necessarily reflect those of the European Communities.

# References


Amboss, K. A.: 1993, A review of the theory of space charge limited operation, *Proceedings of the Conference on Electron Beam Melting and Refining State of the Art 1993, Reno, NV, November 3–5*, pp. 117–126.

Anderson, J. P., Korbly, S. E., Temkin, R. J., Shapiro, M. A., Felch, K. L., and Cauffman, S.: 2002, Design and emission uniformity studies of a 1.5-MW gyrotron electron gun, *IEEE Trans. Plasma Sci.* **30**, 2117–2123.

Anderson, J. P., Temkin, R. J., and Shapiro, M. A.: 2005, Experimental studies of local and global emission uniformity for a magnetron injection gun, *IEEE Trans. Electron Dev.* **52**, 825–828.

Borie, E. and Horcher, U.: 1997, Effect of surface roughness on the velocity spread in electron guns for gyrotrons, *Int. J. Infrared and Millimeter Waves* **18**, 577–594.

Borie, E., Illy, S., and Westermann, T.: 1997, Use of the BFCPIC and BFCRAY to describe space charge limited emission in electron guns for gyrotrons, *Int. J. Infrared Millimeter Waves* **18** 1–22.

Birdsall, C. K. and Langdon, A. B.: 1985, *Plasma Physics via Computer Simulation*, McGraw-Hill Book Company, New York.

Edgcombe, C. J.: 1995, Sources of velocity spread in electron beams from magnetron injection guns, *Int. J. Infrared and Millimeter Waves* **16**, 83–97.

En-Qiu, Zh.: 1985, Thermionic emission from dispenser cathodes, *Int. J. Electronics* **58**, 141–149.

Freeman, J.C.: 2001, Preliminary Study of Electron Emission for use in PIC Portion of MAFIA, *NASA/TM-2001-210890*, pp. 1–67.

Gilmour, A. S.: 1986, *Microwave Tubes*, Artech House Publishers, Boston, MA.

Glyavin, M. Yu., Goldenberg, A. L., Kuftin, A. N., Lygin, V. K., Postnikova, A. S., and Zapevalov, V. E.: 1999, Experimental Studies of Gyrotron Electron Beam Systems, *IEEE Trans. Plasma Sci.* **27**, 474–483.

Goplen, B., Ludeking, L., Smithe, G., and Warren, G.: 1995, User-configurable MAGIC for electromagnetic PIC calculations, *Computer Phys. Communications* **87** 54–86.

Hawkes, P. W. and Kasper, E.: 1989, *Principles of Electron Optics*, Vol. 1, Academic Press, London & San Diego.

Hayashi, Y., Flechtner, D., and Hotta, E.: 2002, Characteristics of electron emission from PZT ferroelectric cathode under strong accelerating field, *J. Phys. D: Appl. Phys.* **35**, 281–286.

HeatWave Labs, Inc.: 2001, Emission characteristics for scandium type dispenser cathodes, *Technical Paper* TB-119 – available online at: http://www.cathode.com/pdf/TB-119.pdf.

Herrmannsfeldt, W. B.: 1988, EGUN—An Electron Optics and Gun Design Program, *SLAC Report-331*, Stanford Linear Accelerator Center.

Herrmannsfeldt, W. B.: 1994, Developments in the Electron Gun Simulation Program, EGUN, *SLAC Report-6726*, Stanford Linear Accelerator Center.

Isagawa, S., Higuchi T., Kobayashi K., Miyake S., Ohya K., and Yoshida M.: 1999, Application of M-type cathodes to high-power cw klystrons, *Appl. Surface Sci.* **146**, 89–96.

Ives, R. L., Bui, T., Vogler, W., Nelson, J., Read, M., Shephard, M., Bauer, A., Datta, D., and Beal, M.: 2006, Beam Optics Analysis - an advanced 3D trajectory code, reported on the HIGH ENERGY DENSITY AND HIGH POWER RF: 7th Workshop on High Energy Density and High Power RF, *AIP Conf. Proc.* **807**, pp. 292–298.

Ives, R. L. and Falce, L.: 2006, Improved dispenser cathodes, reported on the HIGH ENERGY DENSITY AND HIGH POWER RF: 7th Workshop on High Energy Density and High Power RF, *AIP Conf. Proc.* **807**, pp. 158–166.

Jensen, K. L. and Cahay, M.: 2006, General thermal-field emission equation, *J. Appl. Lett.* **88**, 154105-1–3.

Jensen, K. L., Feldman, D. W., and O'Shea, P. G.: 2004, The quantum efficiency of dispenser photocathodes: Comparison of theory to experiment, *Appl. Phys. Lett.* **85**, 5448–5450.

Jensen, K. L., Law, Y. Y., and Jordan, N.: 2006, Emission nonuniformity due to profilimetry variation in thermionic cathodes, *Appl. Phys. Lett.* **88**, 164105-1–3.

Jensen, K. L., Law, Y. Y., and Levush, B.: 2000, Migration and escape of barium atoms in a thermionic cathode, *IEEE Trans. Plasma Sci.* **28**, 772–781.

Krasilnikov, M.: 2006, Impact of the cathode roughness on the emittance of an electron beam, *Proceedings of Free Electron Lasers (BESSY, Berlin, Germany, 2006)* pp. 583–586 [modelled as proposed in Lau, Y.: 1987, Effects of cathode roughness on the quality of electron beams, *J. Appl. Phys.* **61**, 36–44].

Kuznetsov, G. I.: 1997, Cathodes for electron guns, *Phys. Scr.* **T71**, 39–45.

Langmuir, I. and Compton, K. T.: 1931, Electrical discharges in gases Part II. Fundamental phenomena in electrical discharges, *Rev. Mod. Phys.* **3**, 191–257.

Lawson, W., Raghunathan, H., and Esteban, M.: 2004, Space-charge limited magnetron injection guns for high-power gyrotrons, *IEEE Trans. Plasma Sci.* **32**, 1236–1241.

Longo, R. T.: 2003, Physics of thermionic dispenser cathode aging, *J. Appl. Phys.* **94**, 6966–6975.

Louksha, O. I., Piosczyk, B., Sominski, G. G., Thumm, M. K., and Samsonov, D. B.: 2006, On potentials of gyrotron efficiency enhancement: Measurements and simulations on a 4-mm gyrotron, *IEEE Tran. Plasma Sci.* **34**, 502–511.

Lygin, V. K.: 1995, Numerical simulation of intense helical electron beams with the calculation of the velocity distribution functions, *Int. J. Infrared Millimeter Waves* **16**, 363–376.

Lygin, V. K., Manuilov, V. N., and Tsimring, Sh. E.: 1999, Non-stationary simulation of the gyrotron intense helical electron beams, *Nucl. Instrum. Meth.* A **427**, 41–45.

Miram, G., Ives, L., Read, M., Wilcox, R., Cattelino, M., and Stockwell, B.: 2004, Emission spread in thermionic cathodes, *Vacuum Electronics Conference, 2004. IVEC 2004. Fifth IEEE International Volume* issue 27–29 April 2004, pp. 303–304.

Nusinovich, G. S. and Botton, M.: 2001, Quasilinear theory of mode interaction in gyrotrons with azimuthally inhomogeneous electron emission, *Phys. Plasmas* **8**, 1029–1035.

Nusinovich, G. S., Vlasov, A. N., Botton, M., Antonsen, T. M., Cauffman, S., and Felch, K.: 2001, Effect of the azimuthal inhomogeneity of electron emission on gyrotron operation, *Phys. Plasmas* **8**, 3473–3479.

Pagonakis, J. Gr. and Vomvoridis, J. L.: 2004 Evolution of an electron beam with azimuthal density nonuniformity in a cylindrical beam tunnel, *IEEE Trans. Plasma Sci.* **32**, 890–898.

Petillo, J., Eppley, K., Panagos, D., Blanchard, P., Nelson, E., Dionne, N., DeFord, J., Held, B., Chernyakova, L., Krueger, W., Humphries, S., McClure, T., Mondelli, A., Burdette, J, Cattelino, M., True, R., Nguyen, K. T., and Levush, B.: 2002, The MICHELLE three-dimensional electron gun and collector modeling tool: theory and design, *IEEE Trans. Plasma Sci.* **30** 1238–1264.

Prudencio, E., Candel, A., Ge, L., Kabel, A., Ko, K., Lee, L., Li, Z., Ng, C., and Schussman, G.: 2008, Parallel 3D Finite Element Numerical Modelling of DC Electron Guns, *SLAC Report-13097*, Stanford Linear Accelerator Center, pp. 1–10.

Raghunathan, H. and Lawson, W.: 2005, The design of space-charge limited magnetron injection guns with control electrodes for gyroklystron applications, *IEEE Trans. Plasma Sci.* **33**, 1366–1371.

Sabchevski, S. P., Mladenov, G. M., and Idehara, T.: 1999, Modelling and simulation of magnetron injection guns for submillimeter wave gyrotrons, *Int. J. Infrared and Millimeter Waves* **20** 1019–1035.

Sabchevski, S. P., Mladenov, G. M., Titov, A., and Barbarich, I.: 1996, Modelling and simulation of beam formation in electron guns, *Nicl. Instrum. Meth. Phys. Res.* A **381** 185–193.

Sabchevski, S., Zhelyazkov, I., Thumm, M., Illy, S., Piosczyk, B., Tran, T.-M., Hogge, J.-Ph. and Pagonakis, J. Gr.: 2007, Recent evolution of the simulation tools for computer aided design of electron-optical systems for powerful gyrotrons, *Computer Modeling in Engineering and Sciences* **20**, 203–220.

Tsimring, Sh. E.: 2007, *Electron Beams and Microwave Vacuum Electronics*, Wiley InterScience, Hoboken, NJ.

van der Geer, S. B.: 2001, The General Particle Tracer Code: Design, Implementation and Application, *PhD Thesis* (Technische Universiteit Eindhoven); see also: http://www.pulsar.nl/gpt.

Yamamoto, S.: 2006, Fundamental physics of vacuum electron sources, *Rep. Prog. Phys.* **69**, 181–232.

Young, L. M.: 1996, PARMELA, *Report LA-UR-96-1835* (Revised April 22, 2003), Los Alamos National Laboratory.